Hybrids based on layered Silicates

Dissertation

zur Erlangung des akademischen Grades
eines Doktors der Naturwissenschaften (Dr. rer. nat.)
im Promotionsprogramm Polymer Science
an der Bayreuther Graduiertenschule
für Mathematik und Naturwissenschaften (BayNAT)
der Universität Bayreuth

Vorgelegt von
Stephan Weiß

geboren in Coburg

Bayreuth, 2013

Die vorliegende Arbeit wurde in der Zeit von Januar 2009 bis Februar 2013 in Bayreuth am Lehrstuhl Makromolekulare Chemie II unter Betreuung von Herrn Prof. Dr. Axel H. E. Müller angefertigt.

Vollständiger Abdruck der von der Graduiertenschule BayNAT der Universität Bayreuth genehmigten Dissertation zur Erlangung des akademischen Grades eines Doktors der Naturwissenschaften (Dr. rer. nat.).

Promotionsgesuch eingereicht am:	02.05.2013
Zulassung durch das Leitungsgremium:	07.05.2013
Wissenschaftliches Kolloquium:	11.06.2013

Amtierender Direktor:
Prof. Dr. F.X. Schmid

Prüfungsausschuß:
Prof. Dr. Axel. H. E. Müller (Erstgutachter)
Prof. Dr. Adreas Fery (Zweitgutachter)
Prof. Dr. Rainer Schobert (Vorsitz)
Prof. Dr. Josef Breu

Für meine wundervolle Familie.

»Nichts schockiert mich. *Ich bin Wissenschaftler*.«

Indiana Jones

»What surprises me most of all in mankind, is that man will lose their health in order to get money and then they lose that money in order to recover their health. At the same time while worrying about the future, they forget to live the present, this way they end up living in neither the present nor the future. They live as if they are never going to die and they die as if they have never lived.«

Buddha

Table of Contents

Summary

Novel hybrid nanoparticles were synthesized based on combinations of various layered silicates as inorganic core and well-defined polymer chains as a shell. In all cases positively charged 2-(dimethylamino)ethyl methacrylate (DMAEMA) was incorporated into the polymeric structure to serve as a firm anchor onto the negatively charged clay surface via electrostatic adsorption.

First, hybrid nanofillers were synthesized to improve the mechanical properties of a homopolymer matrix by combining a shear-stiff synthetic K-hectorite with a tailored surface activity. For this, the synthetic fluorohectorite with very high aspect ratios was organophilized with a specifically designed macroinitiator created by statistical Reversible Addition Fragmentation Chain Transfer (RAFT) copolymerization of DMAEMA and the initator-monomer 2-(2-bromoisobutyryloxy)ethyl methacrylate (BIEM). The copolymer was firmly anchored through multiple cationic charges distributed over the chain while the multiple initiating functions were used to polymerize the monomer of choice via Atom Transfer Radical Polymerization (ATRP). The final hybrid was equipped with a hydrophobic polymeric shell of poly(methyl methacrylate) (PMMA), which enables dispersion in organic solvents. The hybrid particles were compounded into a polymeric matrix of commercial PMMA and tested with regard to its reinforcing properties. The similarity of the polymeric shell to the homopolymer matrix of the chosen sample composite combined with the inherent stiffness of the inorganic core lead to an increase in tensile modulus of up to 84 % at 5% filler content.

Further, patchy hybrid nanodiscs based on natural montmorillonite as core and a shell made from compartments of two different polymers were evaluated as cheap and versatile compatibilizers in an immiscible polymer blend. In a simple one-step modification process a shell comprising patches of either of two polymer species (PMMA and polystyrene, PS), each chosen to be similar in polarity to one of the matrix polymers, was attached to the inorganic core via Coulomb interaction. The behaviour of these particles in a solvent-cast blend of 2:1 PS/PMMA was investigated via transmission electron microscopy (TEM) and dynamic-mechanical analysis (DMA).

Particles were found distributed in both of the blend's domains and at the interface and an improvement of the storage module of 17% was found.

Finally, kaolinite was used as a core to create true hybrid Janus nanodiscs, which were applied for compatibilizing an immiscible polymer blend of 2:1 PS/PMMA. It was possible to create two chemically distinct surfaces on the clay particle by addressing each of its two basal surfaces individually via simple, but selective, surface modification. Two diblock copolymers were used to create the Janus structure, each one with a first block consisting of monomer units bearing the anchoring group for the respective surface and a second block, PS or PMMA, tailored to the polarity of the respective matrix polymer. Thus it was possible to direct the Janus particles straight into the interface between the polymeric domains, visualized by TEM images taken from solvent-cast nanocomposite films.

Zusammenfassung

Die vorliegende Arbeit befasst sich mit der Synthese einer Reihe neuartiger Hybridnanopartikel durch die Kombinationen verschiedener Schichtsilikattypen als anorganischem Kern und wohldefinierter Polymerketten als organische Schale. In allen Fällen wurde positiv geladenes 2-(Dimethylamino)ethylmethacrylat (DMAEMA) in die Polymerketten integriert und diente der festen Verankerung der Ketten auf der negativ geladenen Schichtsilikatoberfläche durch elektrostatische Adsorption.

Als erstes wurden Nanofüllstoffe entwickelt um die mechanischen Eigenschaften einer Matrix aus Homopolymer zu verbessern. Dies gelang durch eine Kombination von außergewöhnlicher Scherfestigkeit eines synthetischen K-Hectorits als Füllstoffs mit einer maßgeschneiderten Oberflächenaktivität. Hierzu wurde ein synthetisch hergestellter Fluorohectorit mit hohem Aspektverhältnis durch einen speziell entwickelten Macroinitiator (MI), hergestellt durch statistische Copolymerisation von DMAEMA und Bromoisobutyryloxyethylmethacrylat (BIEM) mittels Reversibler Additions-Fragmentierungs Kettenübertragungs (RAFT) Polymerisation, selektiv auf den externen Basalflächen organophilisiert. Über die positiven Ladungen mehrerer DMAEMA Einheiten konnte das Copolymer fest auf der Oberfläche des Schichtsilikats verankert werden. Die durch BIEM bereitgestellten Initiatorfunktionen dienten zum Starten der Polymerisation eines ausgewählten Monomers durch Radikalische Atom Transfer Polymerisation (ATRP). Der fertige Hybrid war mit einer hydrophoben Polymethylmethacylat (PMMA) Schale ausgestattet, welche die Dispersion in organischen Lösemitteln erlaubte. Die Hybridpartikel wurden als Füllstoffe mit einer Matrix aus kommerziellem PMMA kompoundiert und auf ihre verstärkenden Eigenschaften geprüft. Durch die Kombination aus einer Schale, die chemisch der Matrix angepasst ist, und der dem anorganischen Kern eigenen Scherfestigkeit konnte eine Verbesserung des Elastizitätsmoduls von 84% erreicht werden bei 5% Füllstoffgehalt.

Des Weiteren wurden neuartige, scheibchenförmige Kern-Schale Nanopartikel auf der Basis von natürlichem Montmorillonit (MMT) als Kern und einer oberflächenkompartimentalisierten Schale als billige und vielseitige Verträglichkeitsvermittler in nicht-mischbaren Polymerblends untersucht. In einer

einfachen einstufigen Modifikation wurde unter Ausnutzung von Coulomb-Wechselwirkungen auf den anorganischen Kern eine Schale aufgebracht, die aus Flicken zweier Polymerarten (PMMA und Polystyrol, PS) bestand. Beide Polymerarten waren so ausgewählt, dass sie jeweils der Polarität eines der Matrixpolymeren gleichen. Das Verhalten dieser Partikel in Polymerblends mit der Zusammensetzung 2:1 PS/PMMA wurde an Dünnfilmen mit Hilfe von Transmissionselektronenmikroskopie (TEM) und Dynamisch-mechanischer Analyse (DMA) untersucht. Die Partikel wurden verteilt auf jeweils beide Domänen und in der Grenzfläche vorgefunden und führten zu einer Verbesserung des Elastizitätsmoduls um 17%.

Letztlich wurde Kaolinit als anorganischer Kern verwendet um echte scheibchenförmige Hybrid Janus Partikel zu generieren. Dies gelang mit Hilfe von einfacher, selektiver Oberflächenmodifikation. Die Partikel wurden anschließend zur Kompatibilisierung eines nicht-mischbaren Polymerblends mit der Zusammensetzung 2:1 PS/PMMA genutzt. Um die Janus-Struktur auf der Schichtsilikat Oberfläche zu erzeugen wurden zwei Blockcopolymere verwendet, bei denen jeweils ein Block dazu diente, spezifisch auf die jeweiligen externen Basalfläche anzudocken und ein weiterer Block (PS oder PMMA) auf die Polarität der Matrix maßgeschneidert war. Dadurch war es möglich die Janus Partikel direkt in die Grenzfläche zwischen den Domänen zu platzieren. Dies konnte in TEM Aufnahmen von aus Lösung gezogenen Dünnfilmen der Nanokomposite visualisiert werden.

Glossary

AIBN	Azobisisobutyronitrile
ATRP	Atom Tansfer Radical Polymerization
BET	Specific surface area according to the equation of Brunauer, Emmett, Teller
BiEM	(2-Bromoisobutyryloxy)ethyl methacrylate
C12-hect	Potassium fluorohectorite with a dodecylamine modified surface
CBPT	2-Cyano-2-propyl benzodithioate
CEC	Cation exchange capacity
CTA	Chain Transfer Agent
δ	Chemical shift (NMR spectroscopy)
D_x-b-S_y	Poly(2-(dimethylamino)ethyl methacrylate)$_x$-*block*-polystyrene$_y$
DCB	Dithionite-citrate-bicarbonate
DCM	Dichloromethane
DI	Deionized water
DLS	Dynamic light scattering
DMA	Dynamic-mechanical analysis
DMAc	Dimethylacetamide
DMAEMA	2-(Dimethylamino)ethyl methacrylate
DMSO	Dimethylsulfoxid
DP	Degree of polymerization
EDTA	Ethylenediaminetetraacetic acid
EDX	Energy dispersive X-ray spectroscopy
GPC	Gel permeation chromatography
^{1}H-NMR	Proton Nuclear Magnetic Resonance Spectroscopy
HDT	Heat distortion temperature
HEMA	Hydroxyethyl methacrylate
hybrid-hect	Potassium fluorohectorite with a polymeric PMMA shell
IR	Infrared spectroscopy
K-hect	Potassium fluorohectorite
LUM	LUMiFuge® 114
MAS	Magic angle spinning
Mg-hect	Magnesium fluorohectorite
MI	Macro-initiator: (poly(2-(2-bromoisobutyryloxy)ethyl methacrylate)-stat-(2-dimethyl(amino)ethyl methacrylate)
MMT	Montmorillonite
M_n	Number average molecular weight
M_w	Weight average molecular weight

MWD	Molecular weight distribution
N_A	Avogadro constant
Na-hect	Sodium fluorohectorite
NMF	N-Methylformamide
O-hect	Potassium fluorohectorite with a macro-initiator modified surface
OS	External octahedralsurface of a kaolinite tactoide
PCM	Poly(3-(2,3-Dihydroxybenzoyloxy) Propyl Methacrylat)$_{46}$-*stat*-(Methyl Methacrylat)$_{466}$
PDI	Polydispersity Index
PDPS	Poly((2-dimethylamino)ethyl methacrylate)-block-polystyrene
PMMA	Poly(methyl methacrylate)
PPE	(Poly(2,6-dimethyl-1,4-phenylene ether)
ppm	Parts per million
ppm	Parts per million
PS	Poly(styrene)
PXRD	Powder x-ray diffraction
RAFT	Reversible Addition-Fragmentation Chain Transfer
RI	Refractive Index
RT	Room temperature (25 °C)
$Ru(bpy)_3^{2+}$	Ruthenium-Tris-2,2'-Bipyridin-Komplex
SAN	Poly(styrene-*co*-acrylonitrile)
SEC	Size Exclusion Chromatography
si-ATRP	Surface-initiated Atom Transfer Radical Polymerization
TEM	Transmission Electron Microscopy
T_g	Glass transition temperature
TGA	Thermogravimetric analysis
THF	Tetrahydrofuran
TMS	Tetramethylsilane
TS	External tetrahedralsurface of a kaolinite tactoide
UV	Ultraviolet
wt%	Weightpercentage

Chapter 1: Introduction

1.1 Layered silicates

In mankind's early history, the utilization of new materials lead to major technological progress, from the stone- over the bronze- to the copper-age, the new materials enabled better tools, better hygiene and better protection and also often decided the fate of civilizations. Modern society in contrast needs highly specialized materials, often tailored to a single task, to face the challenges of its rapidly advancing technological sectors like automotive, aerospace, hygiene, energy and engineering. Living in the age of polymers, there is already a large supply of basic and advanced materials to choose from, but the introduction of nanotechnology, and with it nanoparticles, opened up a vast range of possibilities for better and novel materials, where even the cheapest basic polymers, which make up most of the daily-use items around the world, can be mixed with a small amount of nanosized objects to enhance and alter their properties significantly[1].

Clay minerals have been used since thousands of years by cultures worldwide as ceramics, but due to their manifold other properties, e.g. high water adsorption, capacity for cation exchange, non-Newtonian fluid behavior they found their way into modern applications, like filtration, purification, encapsulation of wastes, drilling and gardening. A recently advanced topic and one of growing interest is their use in polymeric materials as cheap and versatile nanofillers to enhance their toughness, flame retardency and gas barrier properties. All of these properties are a direct result from their unique layered sheet-like structure after which they are named and classified.

Gary W. Beall and Clois E. Powell ask as an introductory question to their book[2]: „Can one imagine the utility of a dispersed-phase reinforcement for polymers that has a thickness of 1 nm, a plate-like morphology with minimal dimensions of 150 to 200 nm, robust with a modulus of 180 GPa, non-toxic [...], a surface area in excess of 750 m^2/g, a charge suitable for altering its hydrophilic balance at will, and a refractive index similar to polymer so that the nanoparticle will appear transparent in the

polymer composite? How difficult would it be to prepare such a particle?" As the authors are discussing naturally occurring layered silicates, this rhetorical question amplifies the potential which lies in these clay minerals found all over the world in sedimentary rocks like bentonites or kaoline.

Layers are held together by van-der-Waals forces, hydrogen bonds and electrostatic interactions forming large stacks (tactoids) in the dry state. Each layer is roughly 1 nm in height and is made up from two different basic building blocks[3], namely $[TO_4]$-tetrahedra and $[M(O,OH)_6]$-octahedra. Most commonly tetrahedral cations are Si^{4+}, Al^{3+} and Fe^{3+}, while octahedra feature Al^{3+}, Fe^{3+}, Mg^{2+}, Fe^{2+} or Li^{+}. Each corner of one polyhedron is occupied by O^{2-}, OH^{-} or F^{-} anions. Tetrahedra are connected via three shared corners and form a two-dimensional hexagonal lattice structure (Figure 1.1). The fourth apical corner acts as connection to the octahedral layer. Octahedra are connected to each other by shared edges and the upper and lower triangular sides of all tetrahedra lie in plane respectively.

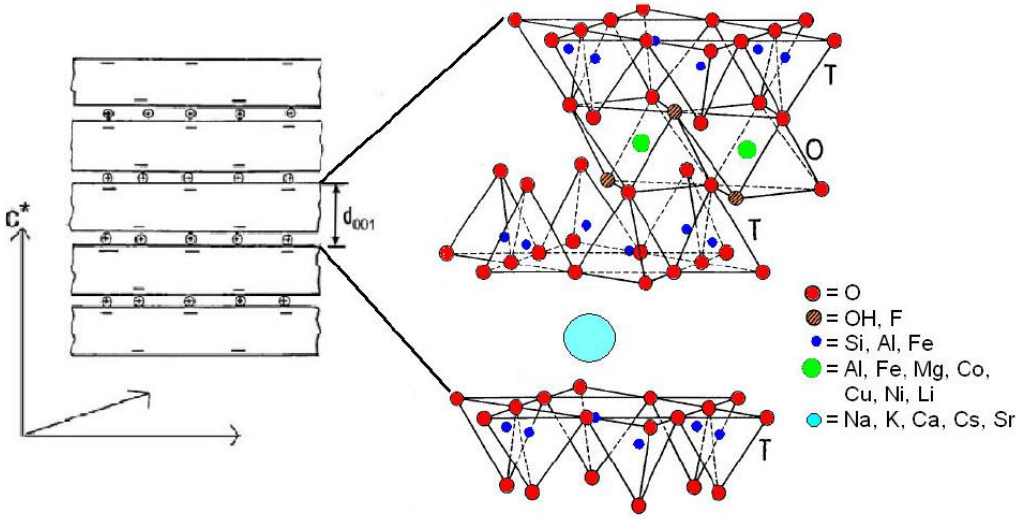

Figure 1.1 Schematic representation of a 2:1 layered Silicate. T= Tetrahedron, O=octahedron. Reprinted with permission from reference [4].

There are two important types of layered silicates, in both cases each lamella consists of one octahedral layer connected either on one side to a tetrahedral layer (named 1:1 layered silicate, e.g. kaolinite, chapter 1.1.3) or sandwich-like on both sides (called 2:1 layered silicate, e.g. montmorillonite or hectorite, chapter 1.1.1 and

1.1.2). This has a major influence on the way how each silicate compensates its layer charge resulting from isomorphous substitution.

Any cation in the tetrahedral or octahedral layer which is replaced by a cation of lower valency will contribute to a permanent net layer charge, ζ, which is compensated by counter-ions close to the layer. The amount of (exchangeable) counter-ions is denoted as cation exchange capacity (CEC). In the case of 2:1 silicates the cations reside on the external basal planes and in the interlayer spaces. The interlayer distance varies with the cation species and its degree of hydration between 9.1 Å and 18.0 Å. A 1:1 silicate does not have any cations in its interlayer space and compensates its charge only at the external tetrahedral layer.

In the case where the open spaces of all octahedrons are filled with cations the layer is called trioctahedral or brucitic (e.g. hectorite, see chapter 1.1.2), while an occupation of only 2/3 is named dioctahedral or gibbsitic (e.g. montmorillonite and kaolinite, chapter 1.1.1 and 1.1.3) (Figure B7c). As a result cations of higher valency (Al^{3+} vs. Mg^{2+}) are incorporated into dioctahedral structures to compensate for the layer charge.

With natural silicates varying degrees of isomorphous substitution occur in each layer, depending on the conditions under which they were formed.

1.1.1 Natural montmorillonite

Montmorillonite (MMT) is a natural 2:1 layered silicate from the smectite group with the dioctahedral structure $(Na, Ca)_{0.3}(Al, Mg)_2(Si_4O_{10})(OH)_2 \cdot nH_2O$. It is found all over the world[5]. It is an alteration product of volcanic tuff and ash, forming bentonite beds, and of wall rocks bordering hydrothermal mineral deposits. It forms under alkaline conditions of poor drainage, with Mg, Ca, Na, and K remaining in the soil. As it is a natural product it contains impurities, most commonly feldspar, quartz, mica, carbonate and hydroxycarbonate, which have to be removed prior to commercial application. Furthermore, all of its properties depend on the conditions it was formed under, varying with its origin. E.g. the CEC reaches from 90 up to 150 meq/100g as the negative charge is distributed inhomogenously inside each layer and between layers, resulting in inhomogeneous surface coverage with counterions,

sometimes resulting in clusters forming around spots with high density of isomorphous substitution[6, 7]. Counterions usually are hydrated sodium or calcium cations, and increasing hydration fosters desaggregation of tactoids and partial exfoliation. Delamination into singular layers of 1 nm height is only observed after ion exchange with Li and removal of amorphous binders. Combined with a lateral dimension of up to over 300 nm, they can reach aspect ratios, α, of up to 300 in theory. Though, these single sheets lose their intrinsic stiffness and start to curl and break under shear (e.g. during mixing), their practical aspect ratio after processing is usually not higher than 100[8].

Nevertheless, due to its easy mining and processing MMT rapidly became the commercially most attractive clay as an additive for polymeric matrices in the last decades and there is a range of companies, supplying MMT with different grades of purity, dimensions and CEC. In its pristine form it is only miscible with hydrophilic polymers, such as poly(ethylene oxide) and poly(vinyl alcohol)[9, 10]. To render MMT miscible with hydrophobic polymers, alkali counterions classically are exchanged with cationic-organic surfactants, such as alkylammonium salts[11, 12].

1.1.2 Synthetic hectorite (Na-fluorohectorite)

Hectorite is a 2:1 layered silicate commonly of the structure $Na_{0.3}(Mg,Li)_3Si_4O_{10}(OH, F)_2$. Natural hectorite belongs to the smectite group as well and is related to montmorillonite, but has a trioctahedral structure.

Its natural variant suffers from the same impurities and inhomogenities described in 1.1.1. To omit those disadvantages, classical solid-state reactions and melt synthesis have been used to produce artificial hectorite. High temperatures lead to statistical distribution of isomorphous substitution, generating a homogeneous layer charge. Until recently this procedure has been very expensive and industrially inapplicable. Development of a new synthetic route in powerful high frequency furnaces by Hussein Kalo at the department of Inorganic Chemistry I of University of Bayreuth under supervision of Prof. Breu allows for production quantities of kilograms with a price of 18 €/kg. But price is not the only benefit; by synthesis it is possible to create much larger platelets, leading to huge practical aspect ratios α of up to 20000 in case

of Li-fluorohectorite or annealed Na-fluorohectorite (hectorite where part of the octahedral O-atoms have been replaced by F-atoms is called fluorohectorite). With homogeneity in surface charge and far less impurities than natural clay[13] it is possible to control alternation between a highly hydrated 'shear-labile' state and a nonhydrated 'shear-stiff', mica-like state by simple cation exchange. This transition between hydration states cannot be observed for natural MMT due to heterogeneity of charge density and lower layer charge. Cation exchange toward Mg-fluorohectorite gives a highly hydrated and therefore 'shear-labile' state, enabling exfoliation by application of shear forces in a stirred media mill[14]. A subsequent cation exchange with K^+ ions yielded a collapsed non-swollen, 'shear-stiff´, mica-like material. Powder x-ray diffraction (PXRD) measurements showed that collapsed stacks will not exchange interlayer cations and thus reactivity is restricted to external basal planes. This prevents the curvature observed in delaminated single sheets and should substantially increase potential reinforcement effects[15].

These unique properties have led to a renewed academic interest to develop hybrid materials based on synthetic hectorite for industrial applications.

1.1.3 Natural kaolinite

Kaolinite is a 1:1 silicate, with the formula unit of $Al_2Si_2O_5(OH)_4$. Tactoid height ranges from 70 nm to 100 nm and lateral extension varies between 500 nm and 15 µm, depending strongly on its origin. Kaolinite has several features not found in 2:1 silicates. Single lamellae in tactoids are not held together by van-der-Waals forces but by strong hydrogen bonds between µ-hydroxide-groups of the octahedral layer and the silicon network of the tetrahedra (Figure 1.2)[16], resulting in much smaller interlamellar distances of 7.2 Å. This makes intercalation difficult and restricts it to only a small range of neutral molecules with high dipolar moments like Dimethyl sulfoxide (DMSO)[17] and N-Methylformamide (NMF)[18].

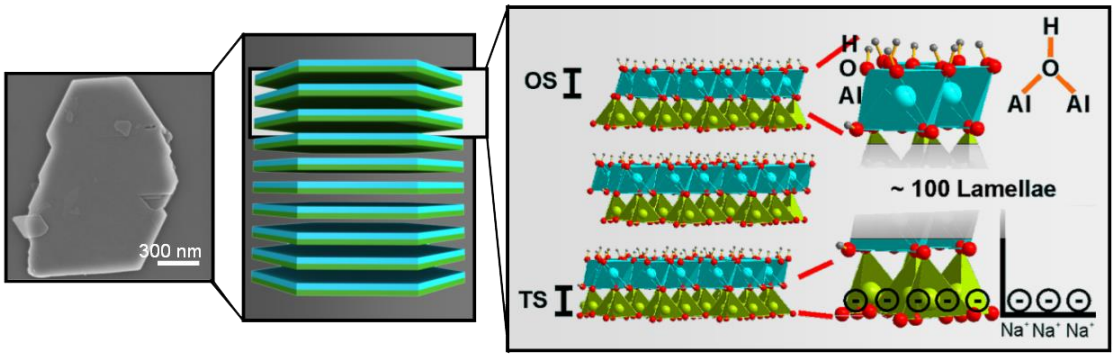

Figure 1.2 Schematic represantation of 1:1 layered silicate (kaolinite). OS= Octahedral surface, TS= tetrahedral surface. Reprinted with permission from reference [14].

The most interesting feature in the particle architecture is the preservation of its polar lamellar structure throughout the tactoid, which means each particle has two chemically distinct surfaces, which can also be selectively targeted for modification to create Janus structures (see chapter 1.2.3).

A combination of both features (no intercalation and chemically distinct external surfaces) leads to the interesting fact that the negative charge generated by isomorphous substitution of Si^{4+} against Al^{3+} in the tetrahedral layer can only be compensated by counterions at the tetrahedral surface (abbreviated TS), which means the outermost tetrahedral layer of a tactoid[19, 20]. Natural counter ions are sodium and calcium, which are easily replaced by other ions respective to their comparatively low CEC, which lies at ~2.6 meq/100g.

Recent studies show that the octahedral layer can be selectively addressed by molecules bearing a catechol moiety[21]. Those groups most likely will undergo a condensation reaction and bind covalently to the μ-hydroxide groups of the octahedral surface (called OS), similar to what was observed with alcohols and structurally related aluminum oxide surfaces[22, 23].

1.2 Organic/inorganic hybrid nanoparticles

Nanomaterials have, by definition, at least one dimension in the nanometer scale (<100 nm) and show novel properties strongly influenced by the large surface to

volume ratio. The synthesis, characterization, and applications of nanoparticles are among the most important sections of the wide range of nanotechnology. In recent years, nanoparticles have gained tremendous attention as the transition from microparticles to nanoparticles was seen to lead to immense changes in the physical and chemical properties of a material. Due to the vast increase in surface area to volume ratio gained from this step down in length scale, surface atoms and their effects now play a dominant role over bulk atoms. Especially when introduced into composites, the huge specific interphase area alters the properties of the matrix considerably.

Research started in the 1980s with nanoparticles made from one material[24-26], but it was quickly discovered, that adding a shell around the core particle gives rise to new materials only possible by combination of both properties[27-29]. The name "core/shell" particles was adopted for materials consisting of a inorganic/organic core of different shapes and an inorganic or organic shell. Applications are manifold[30] and advances in surface modification techniques allow for ever new combinations of core properties and shell properties. A recent example for the multifunctionality of inorganic core/ polymeric shell hybrids are superparamagnetic and fluorescent CdSe(ZnS) nanoparticles coated with protective silica and bearing a polymeric thermo-responsive poly(N-isopropylacrylamide) shell[31].

1.2.1 Clay based hybrid nanoparticles

Clay particles are well suited inorganic cores for the creation of hybrid particles. Even the symmetrical 2:1 structure of smectites already provides two chemically different reactive sites for attaching a shell: basal surfaces and edges. The previously described inherent negative layer charge of layered silicates enables facile modification of the basal surface and interlayer spaces with organic molecules bearing a positively charged group by simple cation exchange. Modification of edge located silanol groups with silicon halides, acid halides or silazanes leads to stronger covalent bonds. Both sites can be accessed to go beyond simple alkyl ammonium surfactant modification by attaching polymers with tailored properties via controlled polymerization of suitable monomers and chain length. Classically smectite-based

hybrid nanoparticles are implemented into polymeric materials to enhance toughness, flame retardancy and gas barrier properties.

1.2.2 Patchy nanoparticles

For mixtures of polymer species of different polarity it is energetically favourable to segregate and form domains of their single polymer species, respectively. If bound to an inflexible core, complete phase segregation becomes inherently difficult and formation of compartmentalized (patchy) shells can be observed.

There has been a recent breakthrough in creation of multicompartment micelles by hierarchical self-assembly of ABC triblock terpolymers[32] and patchy wormlike crystalline core micelles made from ABC triblocks with crystallisable core[33]. These groups report on the potential of patchy particles for hierarchical step-growth polymerization of multicompartment micelles into "micron-scaled segmented supracolloid polymers"[32] and their use as super surfactants close to pure Janus colloids in surface activity, while usually being less complicated to produce.

On the core/shell particle side there are few examples utilizing the promising potential of a patchy shell. Furthermore, most of the produced patchy particles are spherical in nature[34].

As shown by Schmelz et al. patchy particles made from triblock terpolymers with crystallized middle block act as giant surfactants in mixtures of immiscible fluids, reducing the surface tension with an effect comparable to that of Janus cylinders[35]. In this thesis we use disc-like montmorillonite 2:1 layered silicates as core to investigate the influence of a patchy shell on its interfacial behavior in an immiscible polymer blend.

1.2.3 Janus nanoparticles

Particles which embed exactly two distinct sides or surfaces of different chemical property and/or polarity into one structure are called Janus particles, named after the Roman god Janus with two faces and whose name is used symbolically for entities showing character or behavior of two incompatible sides. This non-centrosymmetric appearance leads to a unique set of characteristics regarding

material properties and self-assembly behavior[36]. A whole spectrum of different Janus particle architectures is known. Janus particles can be categorized according to their dimensions. There are three-dimensional spherical particles, two versions of two-dimensional disc-like structures and two different one-dimensional cylinders. While their overall geometry can be simple and symmetric, the lack of chemical centrosymmetry proved to be the biggest challenge in their preparation.

The pioneers in the field of Janus particles were Casagrande and Veyssié. They embedded half of a mesoscopic glass bead into a substrate and then silylated the other half. As the amount of particles producible by those syntheses was very limited, all their methods had the major drawback that they were not applicable on a larger scales[37, 38]. Recently the application of photopolymerization and photolithographic polymerization to microfluidic devices enabled an even higher degree of control and structural variety. The microfluidic device sends a two-phase stream into a channel. There it is cut into droplets by an aqueous crossflow, containing surfactants to stabilize the resultant particles. Then a photopolymerization locks the shape of the biphasic particles. Unfortunately this method is not able to create particles with submicron dimensions yet[39]. Another interesting approach was developed by Müller and coworkers[36] , using the self-assembly behavior of triblock terpolymers. Triblock polymers with phase-separating outer blocks will undergo self-assembly upon film casting and form nanometer-scaled bulk structures, which can be locked by crosslinking the inner part (in this case polybutadiene). Upon dissolution of the polymer, the crosslinked part will preserve its bulk shape and thus will yield non-centrosymmetric particles. By defined engineering of the terpolymer composition the bulk structure and thus the resulting particle shape and size can be controlled.

All these approaches have in common, that they start with symmetrical systems and break those apart into non-symmetrical particles or complicatedly synthesize non symmetrical building blocks to start with instead of applying intrinsically polar particles like kaolinite. As described in chapter 1.1.3 it is possible to address each side individually in solution, facilitating the creation of disc-like Janus particles based on a layered silicate, even in large quantities.

Several fields of application result from the unique structural properties of Janus particles. They have evoked great academic interest, as they represent a class of particles with extraordinary self-assembly behavior. Fundamental understanding of self-assembly processes is attributed with the possibility to create new functionalities not present in the individual building blocks by assembling them into hierarchical superstructures. Their enormous surface activity puts them into the focus of industrial applications as super-surfactants and structuring agents in polymer blends. Furthermore the anisotropic character of single Janus particles is used for optical and analytical probes in confined space [40, 41], medical sensors for cell targeting[42] and switchable electro-optical devices[39].

.

1.3 (Clay reinforced) nanocomposites

The commercial breakthrough of clay reinforced nanocomposites happened in the early 1990´s when Toyota researchers published their work on nylon-6-clay thermoplastic nanocomposite technology[43, 44]. The key aspect was a fundamental improvement of properties at minimal loading. At only 4.2 wt% clay the modulus doubled, strength increased by 50 % and the heat distortion temperature (HDT) increased by 80 °C compared to neat polymer. Toyota still holds a broad range of patents in this technological field. Nevertheless academic and industrial interest is still strong and research and development of clay reinforced nanocomposites is growing.

For most applications it is necessary to organophilize the clay surface to increase the compatibility with the matrix and enable a good dispersability. A well known commercial brand of organophilized MMT is the Cloisite product family by Rockwood Additives, which has been optimized for application in aliphatic polymer matrices. On their product webpage it is claimed that their clay based products can act as a new flame retardant approach, increase modulus and tensile strength, improve barrier properties, increase dimensional stability, are thermoplastic recyclable, improve clarity, increase HDT, reinforce and lower density[45], while at a much lower loading (3-5 wt%) compared to conventional fillers (20-60%). However, as most of

these benefits are a result of large practical aspect ratios they strongly depend on the composite preparation and nanofiller – matrix interaction as detailed in the next chapter.

1.3.1 Nanocomposites based on homopolymers

Addition of layered silicates to polymer matrices can result in great improvements of not only mechanical properties. Depending on compatibility and mixing conditions, the clay tactoids can have different degrees of exfoliation and, thus, aspect ratio, stiffness and dispersion will vary. Organophilization through cation exchange with organic molecules increases interlayer space and decreases electrostatic interactions between layers and thus helps to separate the single sheets of one tactoid from another through shear forces. High compatibility and interaction between surface and matrix will keep the layers from re-aggregating and reduce probability of fatigue cracks at interfaces during stress[46].

With natural clays, the key component to harness all beneficial properties of a nano-scaled well dispersed filler is surface modification. Only with synthetic hectorite, as described in chapter 1.1.2 it is possible to tune inherent stiffness and aspect ratio beyond what is possible with natural clay. By organophilization it is possible to achieve high degrees of exfoliation and dispersion, while at the same time modification with classical surfactants is known to decrease interaction between particle and matrix[4]. But for maximum energy transfer from matrix to filler strong interactions between both are necessary. Together with novel approaches to surface modification by polymer chains it should be possible to realize well dispersed, interacting, shear-stiff, high-aspect ratio nanofillers.

1.3.2 Nanocomposites based on polymer blends

Blending of polymers has become a successful way of delivering affordable materials with properties easily tailored to technical applications, not available by the use of single polymers[47].

Due to the incompatibility between polymeric phases of different polarity in a blend, micron sized phase separation resulting from high interfacial tension has to be

overcome by addition of compatibilizers like surfactants, diblock copolymers or triblock copolymers[47]. To minimize interfacial tension a compatibilizer made from two building blocks of different polarities similar to the ones of the polymer phases is advantageous[48].

Natural, unmodified clay layers are generally hydrophilic due to hydrated counterions and thus incompatible with hydrophobic polymers. They are not particularly suited as compatibilizers for polymer blends as agglomeration and phase separation do not improve the shape of the interface and the domain sizes.

Concerning polymer blends of mixed polarity, with one hydrophilic and one hydrophobic phase, classical organoclay, such as the Cloisite® series, homogeneously surface-modified with alkyl chains, may show favourable interaction with one polymer component, yet unfavourable with the other. In that case the compatibilizing effect depends on the relative strength of the interaction parameter, χ, and thus on polymer composition[49]. In several examples from literature it avoided the hydrophilic one and concentrated in the hydrophobic phase showing weak interfacial activity[50-52]. Such particles will still contribute a reinforcing effect if dispersed well in one phase compared to an unmodified blend.

A Janus particle where one side of the surface is tailored to be favourable for one component and the other side for the other component tends to stay in the interface, minimizing the free energy, reducing domain size and interfacial tension significantly[36]. However, modifying anisometric particles with isotropic surface to obtain Janus character is not trivial and has not been reported for smectites yet.

1.4 Motivation and objective of this thesis

The field of nanoparticles is of outstanding academic and industrial interest as nanotechnological achievements already impact the development of sensors, materials and even medicine. They will continue to shape technological advancement, and breakthroughs on the nanolevel might lead to inventions people thought to be impossible. However there is still a long way to go and science is still at the beginning of understanding all the phenomena related to matters on the

nanoscale. As mentioned previously, transition from microparticles to nanoparticles was seen to lead to immense changes in the physical and chemical properties of a material. Furthermore the potential of combining fascinating properties, like quantum luminescence, magnetism, and many more of inorganic matter with the tunable responsiveness and tailored compatibility with technical and biological environments of organic polymers, seems like an endless playground and able to solve current and future scientific challenges.

The objective of this thesis was to create novel hybrid nanoparticles and apply them in the field of polymer nanocomposites. For that, three types of layered silicates with exceptional properties were used as the inorganic disc-like shaped core of the respective hybrid particle. Combined with the expertise on controlled polymerisation it was possible to create polymeric shells tailored to the task at hand.

Chapter 2: Experimental Part and Methods

2.1 Materials

Synthetic Na-fluorohectorite (Na-hect) with an idealized chemical formula unit $Na_{0.5}[Mg_{2.5}Li_{0.5}]Si_4O_{10}F_2$ was prepared via melt synthesis according to literature[13]. The clay has a CEC of 110 mequiv/100 g, as determined by applying the copper complex ([Cu(trien)]2+) method.[53]

Natural MMT (PGV from Nanocor®) was purified in a four-step procedure including the removal of carbonates and magnesium, deferration and ozonization. Therefore, the clay mineral was stirred in a Na_2H_2EDTA solution (0.1 M) at 55 °C for two hours and the precipitate centrifuged three times at 3500 rpm for 10 min to remove the EDTA complex. Magnesium was removed at pH 8 using the same procedure. Ferrous impurities (amorphous binders) were extracted by adding $Na_2S_2O_4$ to a solution of Na-citrate (0.3 M) and $NaHCO_3$ (1 M) and stirring for 1 hour at 80 °C. Flocculation of the mineral platelets was promoted by adding NaCl. The precipitate was washed with water and centrifuged at 2000 rpm several times. Finally, organic compounds were removed by fluxing the MMT solution with ozone for 6 h.

Kaolinite (Amazone 88/90) from Brazil was provided by Vale International S.A. (Saint-Prex, Switzerland). The mineral was size fractioned by a hydrocyclone but no dispersing agent and no sedimentation agent were added. The kaolinite was further purified by removal of calcium- and magnesium-carbonates with ethylenediaminetetraacetic acid (EDTA), followed by deferration via the dithionite-citrate-bicarbonate (DCB)-method. Moreover ozonisation was applied for 2 hours to remove organic impurities. The particle size of the material was fractionated to < 2 µm by the Atterberg procedure to remove traces of agglomerates. This material was used in characterization experiments. Size fractionated kaolinite < 500 nm was used in blending experiments. Purity of the kaolinite was confirmed applying powder X-ray dif-fraction (PXRD), solid-state nuclear magnetic resonance (NMR) spectroscopy, infrared (IR) spectroscopy, and energy dispersive X-ray spectroscopy (EDX).

2-Cyano-2-propyl benzodithioate (CPBT) (97%, Aldrich), 2-bromoisobutyryl bromide (98%, Alfa-Aesar), triethylamine (min. 99%, Aldrich), 2-hydroxyethyl methacrylate (HEMA) (97% Aldrich) and N,N,N',N'',N''-pentamethyldiethylenetriamine (PMDETA) (97%, Aldrich) were used as received without further purification. Ethyl 2-bromoisobutyrate (EBiB) (99%, Aldrich) was used as sacrificial free radical initiator. Azobisisobutyronitrile (AIBN) (98%, Aldrich) was used after recrystallization twice from methanol. Solvents such as Tetrahydrofuran (THF) (p.a.), Dimethylsulfoxid (DMSO) (p.a.), Dimethylacetamide (DMAc) and anisole (p.a.) were purchased from Aldrich and used as received unless stated otherwise. Dichlormethane (p.a. Aldrich) was stored over molecular sieves (4 Å) to remove water traces. 2-Dimethyl(amino)ethyl methacrylate (DMAEMA) (98% Aldrich), styrene (99% Aldrich) and methyl methacrylate (MMA) (99% Aldrich) were passed over a basic alumina column to remove stabilizer prior to polymerisation. 2-(2-Bromoisobutyryloxy)ethyl methacrylate (BIEM) was synthesized according to literature[54]. Copper bromide (98% Fluka) was purified according to the method described by Keller[55]. MgCl2 and KCl used for cation exchange were purchased from Grüssing GmbH Analytika, Germany.

Poly(methyl methacrylate), PMMA, (M_w = 120,000 g/mol) and polystyrene, PS, (M_w = 192,000 g/mol) were purchased from Sigma Aldrich and used without any further treatment. THF was dried by distillation over Na, and dichloromethane (DCM) was dried by distillation over CaH_2 under an argon atmosphere.

2.2 Instrumentation

2.2.1 Nuclear magnetic resonance spectroscopy (NMR)

Liquid ^{1}H-NMR spectra were recorded under ambient conditions on a Bruker Avance 300 spectrometer. Chemical shifts (δ) are given in parts per million downfield from tetramethylsilane (TMS) as internal standard. The ^{13}C solid-state NMR measurements were performed on a Bruker Avance 2 spectrometer operating at 7.05 T with a resonance frequency ν_0 of 75.468 MHz under magic angle spinning condition (ν_{rot} = 10 kHz) via cross polarization. The ^{13}C spectra were referenced relative to TMS.

2.2.2 Size exclusion chromatographie (SEC)

The molecular weights and molecular weight distribution of the polymers were measured by SEC. Column set: 5 µm SDV gel, 102, 103, 104, and 105 Å, 30 cm each (PSS, Mainz). Used detectors are refractive index (RI) and ultraviolet (UV) operated at 254 nm. Polystyrene standards (PSS, Mainz) with narrow molecular weight distribution were used for calibration of the column set, and tetrahydrofuran (THF) and Dimethylacetamide (DMAc) were used as eluents at a flow rate of 1 ml/min.

2.2.3 Transmission electron microscopy (TEM)

The polymer/hybrid thin films were cut with a Leica EM UC7 microtome and TEM images were recorded with a Zeiss EM 922 Omega microscope at 200 kV.

2.2.4 Scanning electron microscope (SEM)

The scanning electron microscope (SEM) images were recorded with a field-emission LEO Gemini microscope 1530 (Zeiss) with an acceleration of 2 kV equipped with a field emission cathode. The films were mounted on a sample holder and sputtered with platinum.

2.2.5 Thermogravimetric analysis (TGA)

TGA was carried out using a Mettler Toledo TGA/SDTA 85 at a heating rate of 5 K/min between 30 and 700 °C under air-flow of 60 ml/min. The typical sample weight was between 8 and 15 mg.

2.2.6 Dynamic light scattering

DLS experiments were carried out to determine the hydrodynamic radii of the polymers. For that purpose an ALV DLS/SLS-SP 5022F compact goniometer system with an ALV 5000/E correlator and a He-Ne Laser (λ = 632.8 nm) at 25°C was used. Before the experiment, the solution (concentration of 1 g/l) was filtered through a Millipore syringe filter with pore size of 0.45 µm. Resulting intensity autocorrelation functions were processed by CONTIN-analyses and the apparent hydrodynamic radii were calculated using the Stokes-Einstein-relation.

2.2.7 Stability measurements (LUMiFuge®)

The stability measurements were performed in a LUMiFuge® 114 (LUM) with a variable rotation frequency of 300, 600, 900 rpm (rounds per minute) and different time intervals of 200 s, 300 s, and 900 s, respectively. Kaolinite suspensions (0.25 wt%) in THF and water were placed in tubes in horizontal positions on the disc of the LUMiFuge®. During the horizontal rotation of this disc the transparencies of the suspensions were measured in the area between the menisci and the sediment. The mean transparency of the whole area was determined. The transparency was measured in time intervals of 10 s while increasing rotation speed stepwise. High turbidity, even after applying centrifugal forces indicates a stable suspension.

2.2.8 Charge titration stability analysis (Stabisizer®)

Determination of point of zero charge of the clay platelets was done using a Stabisizer® (Particle Metrix GmbH). Therefore the microionic clouds of localized particles are displaced by flow induced via a piston. The generated potential is measured and used for monitoring titration with mono- and polycationic species. After complete replacement of displaceable sodium ions by immobile cations the point of zero charge is reached. Four separate solutions containing the polycationic MI solution (1 g/l) in deionized water (DI) were prepared with different pH values using acetic acid (100 %) in order to protonize the amine functions. The point of zero charge for the clay basal surface was measured using a charge titration stability analyzer.

2.2.9 Dynamic-mechanical analysis (DMA) and tensile tests

Dynamic-mechanical analysis (DMA) experiments are carried out in the tension mode at a constant force of 5 N and a temperature range from 30 to 140 °C using a Mettler Toledo DMA/STDA 861e. The heating rate is 5 °C/min and the test specimens is approximately 25 mm in length, 6 mm in width and 1 mm in thickness.

Tensile modulus, tensile strength and elongation at break were measured using a Universal Tensile Tester according to ISO 527 applying a strain rate of 1 mm/min. For

each material at least 8 samples were tested. The elongation at break was determined by a macro-displacement-transducer.

2.2.10 Powder X-ray diffraction (PXRD)

The powder X-ray diffraction (PXRD) patterns were recorded in reflection mode using nickel filtered Cu-Kα radiation λ =1.54187 Å on a Bragg-Brentano-geometry diffractometer (PANalytical Xpert-Pro) equipped with an X'Celerator Scientific RTMS detector.

2.2.11 Fourier-transform infrared spectroscopy (FT-IR)

The particles powders of untreated and treated clay were characterized with a Nicolet FTIR 460 (Thermo Nicolet Corp.). The transmittance absorption spectra were scanned 64 times at 4 cm^{-1} spectral resolution at room temperature.

2.2.12 Specific surface area measurements

The specific surface area of a freeze-dried K-hect sample was calculated from the N2 adsorption/desorption isotherms using the Brunauer-Emmett-Teller (BET) equation. Measurements were carried out on a Quantachrome Nova 2000e analyzer.

2.3 Tailoring of stacks height and stiffness of fluorohectorite

The aqueous dispersion of synthetic Na-hect was transferred to a highly hydrated 'shear-labile' state by exchanging the interlayer Na^+ with Mg^{2+} cations (Mg-hect). The aqueous dispersion of Mg-hect was processed in a stirred media mill (LabStar LS1) for 60 minutes in order to exfoliate the tactoid stacks by applying shear forces. The degree of exfoliation was controlled by the number of milling passages[14]. Subsequently, the clay was transferred into a collapsed and non-swollen 'shear-stiff' mica-like material (K-hect) with no intracrystalline reactivity by exchanging Mg^{2+} with K^+ cations[56]. All exchanging procedures were followed by washing several times with water to remove chlorine ions.

2.4 Synthesis of the copolymers for surface modification

2.4.1 Synthesis of the catechol-modified PMMA copolymer (PCM)

3,4-Dibenzoxybenzoic acid **1** and 3-hydroxypropylbenzoate **2** were prepared following literature procedures (scheme 5.1).[57]

*3-Methacryloyloxypropyl-3,4-dibenzoxybenzoate **3***

Compound **2** (2.11 g, 5.38 mmol) was dissolved in dry DCM (20 ml) and cooled in an ice bath. Et_3N (1.12 ml, 8.07 mmol) and methacryloyl chloride (626 µl, 6.47 mmol) were added and the reaction mixture was stirred at room temperature for 3 h. After washing with water the aqueous phase was extracted with DCM and the combined organic phases were dried over Na_2SO_4, filtered and concentrated in vacuum. The residue was purified by column chromatography (silica gel 60, ethyl acetate/*n*-hexane 1:2, v/v). Yield: 1.64 g (3.57 mmol, 67%); colorless oil; R_f = 0.63 (ethyl acetate/*n*-hexane 1:2); ν_{max} (ATR)/cm^{-1}: 3032, 2963, 1711, 1636, 1599, 1510, 1454, 1427, 1380, 1321, 1266, 1204, 1163, 1130, 1104, 1038, 1006, 944, 815, 761, 734, 695; ^{1}H NMR (300 MHz, $CDCl_3$): δ 1.92 (3 H, s), 2.0-2.2 (2 H, m), 4.28 (2 H, t, ^3J 6.3 Hz), 4.36 (2 H, t, ^3J 6.3 Hz), 5.18 (2 H, s), 5.21 (2 H, s), 5.5-5.6 (1 H, m), 6.0-6.1 (1 H, m), 6.91 (1 H, d, ^3J 9.0 Hz), 7.3-7.5 (10 H, m), 7.6-7.7 (2 H, m); ^{13}C NMR (75.5 MHz, $CDCl_3$): δ 18.3, 28.2, 61.3, 61.4, 70.8, 71.2, 113.2, 115.6, 123.0, 124.0, 125.6, 127.1, 127.4, 127.9, 128.0, 128.5, 128.6, 128.9, 136.2, 136.5, 136.8, 148.3, 153.0, 166.1, 167.3; *m/z* (%) 461 (13) [M^+], 460 (47) [M^+], 369 (6), 317 (8), 225 (17), 181 (27), 127 (12), 91 (100).

*Copolymer PCBM **4***

Methyl methacrylate (650 mg, 6.52 mmol), compound **3** (100 mg, 0.22 mmol) and dodecanethiol (26 mg, 0.13 mmol) were dissolved in dry THF (3 ml) under argon atmosphere and AIBN (10 mg) was added to the reaction mixture, which was stirred under reflux for 5 h. The solution was poured into cyclohexane (100 ml) and the appearing colorless precipitate was collected and precipitated once more from an acetone/cyclohexane mixture. Yield: 710 mg; colorless solid; ν_{max} (ATR)/cm^{-1}: 2996,

2952, 1722, 1601, 1484, 1448, 1432, 1385, 1363, 1268, 1241, 1189, 1144, 989, 965, 911, 842, 761, 748, 698; ^{1}H NMR (300 MHz, acetone-d_6): δ 0.8-1.0 (33 H, m), 1.8-2.0 (24 H, m), 3.61 (30 H, s), 4.1-4.2 (2 H, m), 4.3-4.4 (2 H, m), 5.2-5.3 (4 H, m), 7.1-7.7 (13 H, m).

*Copolymer PCM **5***

Compound **4** (580 mg) was dissolved in dioxane/methanol (40 ml, 1:1), flushed with argon and 10% Pd/C (80 mg) was added. The argon atmosphere was replaced by hydrogen gas and the reaction mixture was stirred at room temperature for 5 h. The suspension was filtered over celite and the filtrate was concentrated in vacuum. The oily residue was triturated with *n*-hexane and dried in vacuum. Yield: 500 mg; off-white solid; ν_{max} (ATR)/cm^{-1}: 3392, 2996, 2950, 1725, 1605, 1480, 1444, 1386, 1270, 1239, 1191, 1146, 1121, 988, 965, 889, 873, 842, 765, 750; ^{1}H NMR (300 MHz, DMSO-d_6): δ 0.5-0.9 (33 H, m), 1.6-2.0 (24 H, m), 3.55 (30 H, s), 4.0-4.1 (2 H, m), 4.2-4.3 (2 H, m), 6.81 (1 H, d, ^{3}J 7.9 Hz), 7.2-7.4 (2 H, m), 9.32 (1 H, s), 9.81 (1 H, s); ^{13}C NMR (75.5 MHz, DMSO-d_6): δ 16.1, 18.4, 27.5, 43.9, 51.6, 53.7, 60.8, 115.2, 116.3, 120.5, 121.8, 145.0, 150.4, 165.5, 176.2, 176.9, 177.3.

2.4.2 Synthesis of poly(2-(2-bromoisobutyryloxy)ethyl methacrylate)-stat-(2-dimethyl(amino)ethyl methacrylate) (MI) *via* Reversible Addition-Fragmentation Chain Transfer (RAFT) polymerization

To a 100 ml round bottom flask, equipped with rubber septum, 1.7 g (6.1 mmol) of BIEM, 6.7 g (42.8 mmol) of DMAEMA, 270 mg (1.2 mmol) of 2-cyano-2-propyl benzodithioate (CPBT), 100 mg (0.6 mmol) of AIBN, 40 ml of DMSO as solvent and 2 ml of anisole as internal standard were added. After three freeze-pump-thaw cycles the reaction was placed into an oil bath at 70 °C for 4 h to reach a conversion of 54% as determined by ^{1}H NMR spectroscopy. The resulting polymer solution was cooled down, exposed to air and dialysed against dioxane until no monomer related peaks at 5.8-6.4 ppm were detected by NMR spectroscopy. M_n = 9000 g/mol and M_w = 16000 g/mol was determined via SEC with DMAc as eluent and a DMAEMA calibration. The final polymer is from here on referred to as maco-initiator (MI). ^{1}H

NMR (300 MHz, $CDCl_3$, δ in ppm): 4.4 – 4.1 (R-C(-CH_3)-COO-*CH_2*-*CH_2*-OOC-C(CH_3)$_2$-Br), 4.0 (R-C(-CH_3)-COO-*CH_2*-CH_2-N-(CH_3)$_2$), 2.6 (R-C(-CH_3)-COO-CH_2-*CH_2*-N-(CH_3)$_2$), 2.2 (R-C(-CH_3)-COO-CH_2-CH_2-N-*(CH_3)$_2$*), 1.9 (R-C(-C*H_3*)-COO-CH_2-CH_2-OOC-C(*CH_3)$_2$*-Br), 1.8 (R-C(-*CH_3*)-COO-CH_2-CH_2-N-(CH_3)$_2$).

2.4.3 Synthesis of poly(2-(dimethylamino)ethyl methacrylate) (PDMAEMA) based diblocks *via* RAFT

All polymerizations were carried out at 80°C in septum sealed flasks. Detailed amounts of reactants are listed in Table 1. In each case DMAEMA precursors were prepared by placing 1,4-dioxane, DMAEMA, AIBN, the chain transfer agent (CTA), 2-cyano-2-propyl benzodithioate, and 1,3,5-trioxane in the reaction flask. Nitrogen flow was established for 20 min at room temperature and then the polymerization was initiated by heating the flask in an oil-bath. The precursor solution was transferred to a degassed and heated solution of 1,4-dioxane, second monomer and 1,3,5-trioxane after 4h at a typical conversion of DMAEMA of above 90 %. The reaction was terminated by cooling in an ice bath and exposure to atmospheric oxygen. The polymers were purified by precipitation into a non-solvent (isopropanol for PS containing diblocks and cyclohexane for PMMA containing diblocks) and freeze-dried from 1,4-dioxane. Final polymers are abbreviated D_{17}-*b*-M_{300} in the case of poly(2-(dimethylamino)ethyl methacrylate)$_{17}$-*block*-poly(methyl methacrylate)$_{300}$ and D_{17}-*b*-S_{360} in the case of poly(2-(dimethylamino)ethyl methacrylate)$_{17}$-*block*-polystyrene$_{300}$.

Table 1 Applied amounts of chemicals in the preparation of the PDMAEMA-macro-CTA and the diblock-copolymers in 1,4-dioxane .

Formula [a]	DMAEMA / mg, mmol	CTA / mg, mmol	AIBN / mg, mmol	Monomer / g, mmol	Solvent/ ml
D_{17}-*b*-M_{300}	380; 2.5	54; 0.25	15; 0.09	12.0; 120	30
D_{16}-*b*-S_{360}	1083; 6.9	149; 0.67	38; 0.24	35.2; 338	30
D_{16}-*b*-S_{115}	1402; 9.1	100; 0.45	26; 0.18	18.8; 181	30

[a] repeating units of DMAEMA calculated by subtracting the molecular weight of CPBDT (221.00 g/mol) and dividing by the molecular weight of DMAEMA (157.21 g/mol), repeating units of the second block

were calculated by subtracting the molecular weight of DMAEMA block, acronyms: D: DMAEMA, , S: styrene, M: MMA

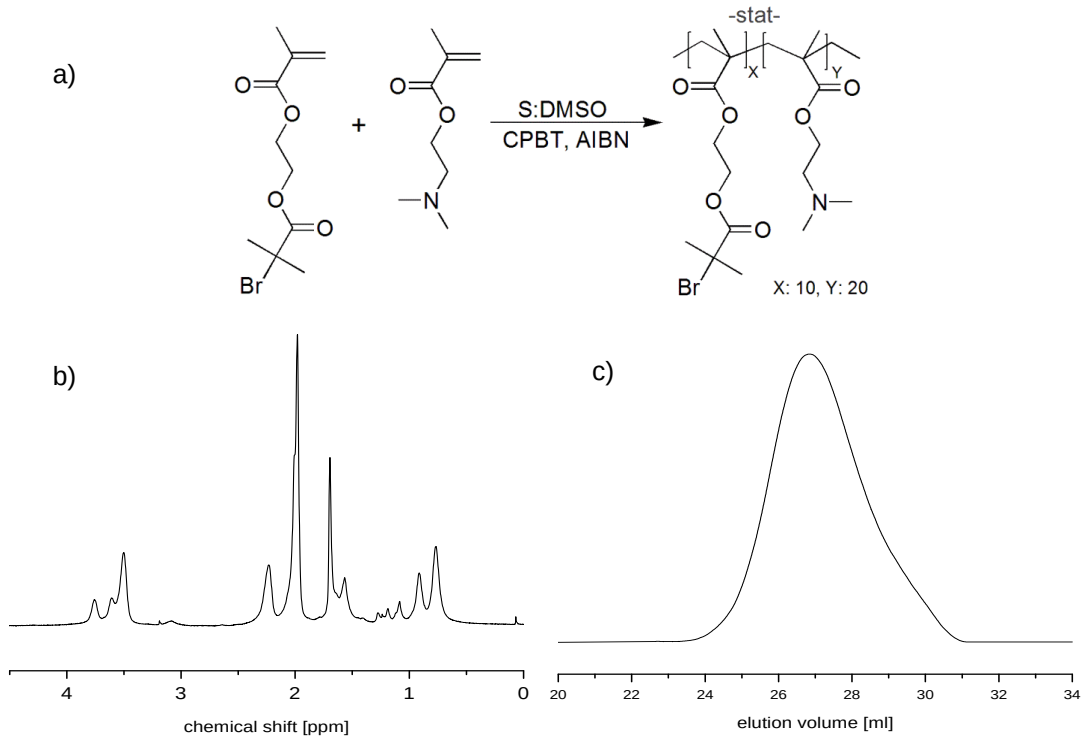

Figure 3.1 a) Synthesis of the statistical copolymer (PDB) and characterization *via* b) ^{1}H-NMR spectrum and c) SEC trace with DMAc as an eluent.

2.5 Clay surface modification

2.5.1 Surface modification of K-fluorohectorite and surface-initiated Atom Transfer Radical Polymerization (si-ATRP) of methyl methacrylate (MMA)

The external surface of K-hect (10 g) was modified with the MI (320 mg) in DI water at pH=6.8. Subsequently, the flocculated hydrophobic nanoplatelets (O-hect) were centrifuged and redispersed in THF. The grafting of MMA was initiated from O-hect *via* a copper mediated ATRP in the presence of EBiB as a free sacrificial initiator. All experiments were performed under inert atmosphere in a conventional run procedure[58, 59]; A dispersion of the O-hect (10 g; calculated 390 µmol of initiating

sites) in 400 ml THF, MMA (164.5 g; 1.462 mol) and EBiB (19 mg; 97.5 µmol) were added to a flask and sealed with a rubber septum. The reaction mixture was degassed three times by freeze-pump-thaw cycles and filled with argon. In a separate flask a stock solution of PMDETA, Cu(I)Cl and $Cu(II)Cl_2$ (338 mg; 975 µmol, 115.8 mg; 1.17 mmol and 39.2 mg; 292.5 µmol) in 20 ml anisole was degassed for 30 min under argon. Finally, 10ml of the stock solution was introduced to the reaction flask by a syringe. The reaction flask was immersed in an oil bath at 80 °C. Samples were withdrawn at various times to monitor the reaction kinetics and it was stopped after 300 min by cooling and exposing to air. The final hybrids of K-hect with a polymeric shell of PMMA chains with an average DP of 380 (hybrid-hect (DP 380)) were centrifuged and washed several times with THF.

As a reference a nanofiller with a commercial surfactant, dodecylamine, was used after protonation using one equivalent of HCl (0.1 mol). Standard procedures were used to exchange the K^+ cations with the organic cation (C12 ammonium chloride)[60]. After ion exchange, the modified nanoplatelets (C12-hect) were centrifuged and washed several times with DI water, ethanol, and THF.

2.5.2 Surface modification of montmorillonite (MMT)

The diblock copolymer solutions of D_{17}-*b*-M_{300} and D_{17}-*b*-S_{360} for surface modification of MMT were prepared in two different ways:

1. Solutions with pre-formed micelles of D_{17}-*b*-M_{300} and D_{17}-*b*-S_{360} were prepared by dissolving the polymer in THF and adding water (pH=6.5) dropwise until turbidity occurred.

2. Molecularly dispersed solutions were prepared by adding the freeze dried polymer into THF and stirring until no solids were visible anymore and the transparent solution had a slightly pink colour.

The polymer solutions (30 mg, 1 mg/mL) were added to a dispersion of MMT in water (100 mg, 5 mg/mL, pH=6.5) using a cannula and stirred over night. Final MMT/PS/PMMA hybrid particles (hybrid-MMT) were purified by removing non-anchored polymer *via* centrifugation at 4000 rpm, decantation of the supernatant and redispersion in water (1x) and THF (3x) using ultrasonication.

2.5.3 Surface modification of kaolinite

It is possible to modify each side, the tetrahedral surface and the octahedral surface (TS and OS), of the kaolinite specifically and individually without influencing the other side as shown in a previous publication[21]. The order of modification chosen, starting with D_{16}-*b*-S_{115} has a purely practical purpose, as the DMAEMA block of the D_{16}-*b*-S_{115} is charged at pH 6 and thus kaolinite can be modified in aqueous suspension where it is dispersed best. After cation exchange the unilaterally modified kaolinite can be dispersed in THF more easily than unmodified kaolinite, as seen in Fig. 5.4 (stability measurements). PCM is soluble in THF, but not in water. Nevertheless pristine kaolinite can be modified by PCM as first step as well, but for that kaolinite has to be dispersed in THF by vigorous stirring first.

Modification of TS

100 mg D_{16}-*b*-S_{115} were dissolved in 30 ml THF. 400 mg of the kaolinite was suspended in 30 ml of water (pH~ 5.5, degree of protonation of the DMAEMA block ~80 %[61]). After 20 min of stirring a complete flocculation of the kaolinite was achieved and the suspension was washed ten times with THF to remove the excess of D_{16}-*b*-S_{115}. The hybrid was dispersed and stored in THF to prevent drying.

Modification of OS

100 mg of PCM was dissolved in 20 ml dry THF under argon atmosphere in a Schlenk flask. 400 mg kaolinite (pristine or already unilaterally modified hybrid) was dispersed in the PCM THF solution by vigorous stirring over night at 60 °C. After the reaction the kaolinite was washed ten times with THF to remove the excess of PCM and then dispersed in THF to give hybrid-kaolinite.

2.6 Preparation of clay/polymer nanocomposites

2.6.1 Embedding of K-fluorohectorite/PMMA hybrid particles (hybrid-hect) into a PMMA Matrix for tensile testing

Two different K-fluorohectorite/PMMA hybrid nanoparticles were evaluated as nanofillers in a PMMA matrix: hybrid-hect (DP 380) and C12-hect were mixed with a solution of PMMA in THF (5 wt. -% clay loading), respectively. To ensure good distribution of the clay in the polymer matrix both dispersions were placed in an overhead shaker overnight. Both dispersions were film casted and dried in a vacuum oven first at 90 °C for 14 h followed by drying at 140 °C for another 18 h. Neat PMMA was treated in a similar way before melt compounding. The dried nanocomposite materials were melt-compounded in a discontinuous counter-rotating twin-screw microcompounder (DSM Xplore, 15 ml microcompounder) at a temperature of 190 °C, a mixing speed of 210 rpm and a mixing time of 3 min. The material was added stepwise to the running microcompounder and during each cycle a batch of 7.5 g was processed. After extrusion, the melt was injection-moulded with a microinjector (DSM Xplore 12 ml injection moulding machine; melt temperature: 190 °C; mould temperature: 40 °C; injection pressure: 8 bar) into dumbbell specimens (75 mm × 5 mm × 2 mm) for tensile testing.

2.6.2 Preparation of hybrid-clay/polystyrene (PS)/PMMA nanocomposite samples for TEM analysis

PS and PMMA in the ratio of 1:2 were dissolved in THF. The polymer content of the solutions was 10 wt%. 50 mg of hybrid-clay (hybrid-MMT or hybrid-kaolinite) was suspended in 10 ml of the PS/PMMA solutions by 15 minutes of strong shearing (Heidolph Silent Crusher, 16.000 rpm) at 30 °C, resulting in 5 wt% hybrid-clay in the final, dry blend.

A film was cast by letting the solvent evaporate slowly from the mixture in a glass vial. The resulting dry film was cut with an ultramicrotome and examined *via* TEM.

2.6.3 Preparation of hybrid-MMT/PS/PMMA nanocomposite samples for DMA

The PS/PMMA matrix containing the hybrids is cast into glass petri dishes and dried in a vacuum oven. The polymer is crushed and melt pressed into DMA mould samples using hot plates from P/O/Weber co. (Germany). The samples are melted at 200 °C without pressure for about 6 minutes, removing last traces of THF, then heat pressed for 5 minutes using 70-75 kN and finally cold pressed for 3 minutes using 30-40 kN.

Chapter 3: Hybrid mica-like particles based on high aspect ratio fluorohectorite

This chapter is the result of an intensive cooperation with Mazen Ziadeh and major parts of this chapter are to be submitted to the Journal of Materials Chemistry under the title: “Tailored Mica-Like Clay / Poly(Methyl Methacrylate) Hybrid Nanofiller Based on High Aspect Ratio Fluorohectorite” by Mazen Ziadeh and Stephan Weiß, Bianca Fischer, Axel H. E. Müller, Volker Altstädt and Josef Breu.

3.1 Preparation of tailored mica-like K-fluorohectorite/PMMA hybrid particles

In contrast to the aforementioned common pathways towards hybrid nanofiller based on (partially) delaminated, surface grafted natural clays, we present a novel strategy yielding ‘shear-stiff’ nanofiller covered with polymer chains of the desired molecular weight preventing any intercalation into the interlayer during the grafting process and thus preserving the aspect ratio.

3.1.1 Tailoring of a high aspect ratio mica-like nanofiller

To harness the advantages of large platelets with homogeneity in surface charge and far less impurities than natural clay[13] a Na-hectorite (Na-hect) was prepared via melt synthesis. The resulting synthetic clay platelets featured large lateral extension and a homogenous charge distribution. The novel Na-hect is an optimal material because it allows for a controlled alternation between highly hydrated, ‘shear-labile’ state and a non-hydrated, ’shear-stiff’, mica-like state by simple cation exchange. This transition between hydration states cannot be observed for natural MMT due to heterogeneity of charge density and lower layer charge. Cation exchange towards Mg-hect gives a highly hydrated and therefore ‘shear-labile’ state, enabling the exfoliation by applying shear forces in a stirred media mill[14]. A subsequent cation exchange with K^+ ions yielded a collapsed non-swollen, ‘shear-stiff’, mica-like material as depicted in Fig. 3.2a. We were able to obtain a rough estimation of the average aspect ratio using a previously introduced method which correlates the

tactoid thickness as determined by the Scherrer equation with the value of the total specific surface area[56]. The high aspect ratio of the nanoplatelets increased the fraction of surface/interface significantly. Thus, by having a median particle size distribution, X_{50}, of 6.4 µm as determined by static light scattering and a large external specific surface area of 68 m^2/g obtained via N_2-adsorption measurement using the BET equation, we can estimate an average aspect ratio of 550.

3.1.2 Selective surface modification of the mica-like nanofiller

The main concern of this study is to produce high aspect ratio mica-like hybrid nanofiller which do not undergo exfoliation during the subsequent polymer grafting from the clay surface. As mentioned before a good interfacial management between filler and matrix is necessary to increase the potential of clay as a reinforcing phase in polymeric nanocomposites. In general, commercially available surfactants provide good adhesion to the clay surface, but cannot generate optimal interaction with a broad range of matrices, due to their limited chemical structure. Polymer chains attached to the clay's surface can provide better interfacial interaction, as they can be tailored to the chemical structure of the matrix polymer by using a similar composition of monomer units. Monocationic initiators are suboptimal for grafting polymer chains from layered silicates, as on the one hand they are able to intercalate between the layer stacks, widen them and make them prone to exfoliation. On the other hand, polymer chains having only one single positive charge have a chance to detach from the clay surface under stress[62, 63]. To optimize the compatibility between nanofiller and matrix a tailor-made polycationic macroinitiator (MI), inspired by the one used by Armes to modify ultrafine inorganic oxide sols[64], was developed. It showed strong adhesion to the surface of the clay due to multiple anchoring groups and is capable to increase the compatibility between nanofiller and matrix since it is bearing multiple initiator groups for a subsequent si-ATRP. The MI used in this study consists of a statistical copolymer of 2-(dimethyl ethylamino)ethyl methacrylate (DMAEMA) and 2-(2-Bromoisobutyryloxy)ethyl methacrylate (BIEM). The ratio was determined via ^{1}H-NMR analysis to be 2:1 on average, and the average chain length according to SEC was 30, yielding around ten potential ATRP initiator functions per MI (Fig. 3.1). Furthermore, by tuning pH one can control the charge

density of the amine groups for optimal adhesion and stability of the MI on clay surface while uncharged amine groups act as neutral spacer (Fig. 3.2 b). In addition, by adjusting the ratio of BIEM to DMAEMA, it is possible to control the grafting density of the resulting polymeric chains.

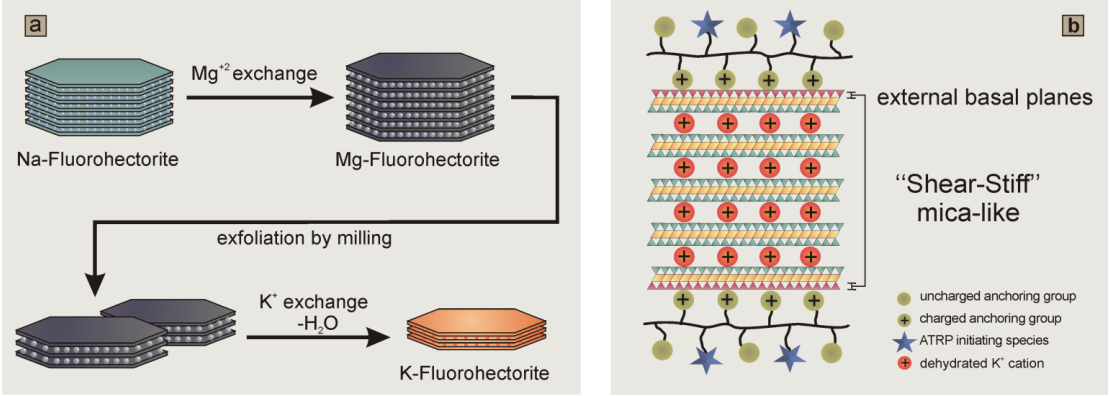

Figure 3.2 (a) A structural scheme of tailoring 'shear-stiff', mica-like platelets with high aspect ratio after exfoliation and exchanging the interlayer cations. (b) Selective modification restricted to external basal planes using MI.

The amount of MI anchored to the external basal surface can be determined by measuring the point of zero charge using a Stabisizer®. To attain different protonation degrees of the amine function of PDMAEMA the pH of the solution was adjusted using acetic acid. The pH dependent titration curves of different aqueous solutions with the same amount of K-hect are shown in Fig. 3.3.

It is clear that adjusting the pH of the solution influences the anchoring density of the MI. With lower pH the degree of protonation increases[61] and therefore less polymer is required to cover the surface and reach the point of zero charge. There is a strong relationship between higher packing density of MI on the external basal surface and the concentration of the initiated grafted PMMA from the stiff surface[65]. The modification of K-hect with MI leads to the organophilization of the clay altering its state from hydrophilic to hydrophobic, leading to flocculation of the platelets in aqueous solution. It is noteworthy to mention that the quality of the dispersion in THF after organophilization is significantly enhanced at higher pH which means more MI being anchored onto the surface. Prior to all polymerizations, modification of K-hect took place at pH=6.8 in order to maximize the amount of initiating groups and

the quality of dispersion in THF. K-hect modified at this pH will be referred to as O-hect hereafter.

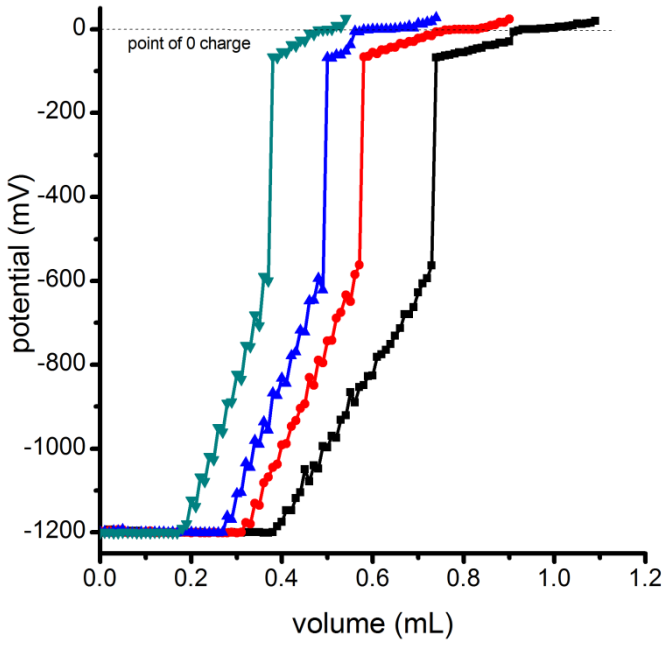

Figure 3.3 Volume of MI (1g/l) needed to achieve point of 0 charge using pH dependent solutions (■) pH: 7.8, (●) pH: 6.8, (▲) pH: 5.7 and (▼) pH: 5.1.

The modified mica-like surface was analysed qualitatively by FT-IR and solid state NMR. Fig. 3.4 illustrates the FT-IR spectra of K-hect and that of O-hect. The K-hect spectrum exhibits peaks for Si-O out-of-plane bending at 708 cm^{-1} and also Si-O stretching band at 970 cm^{-1}. Furthermore, H-O-H bending at 1637 cm^{-1} and a wide vibration of O-H stretching band in the range 3600-3100 cm^{-1} is observed[66]. After modification with MI distinguished peaks that can be assigned to the C=O and C-O vibrations at 1735 and 1216 cm^{-1}, respectively, can be found.

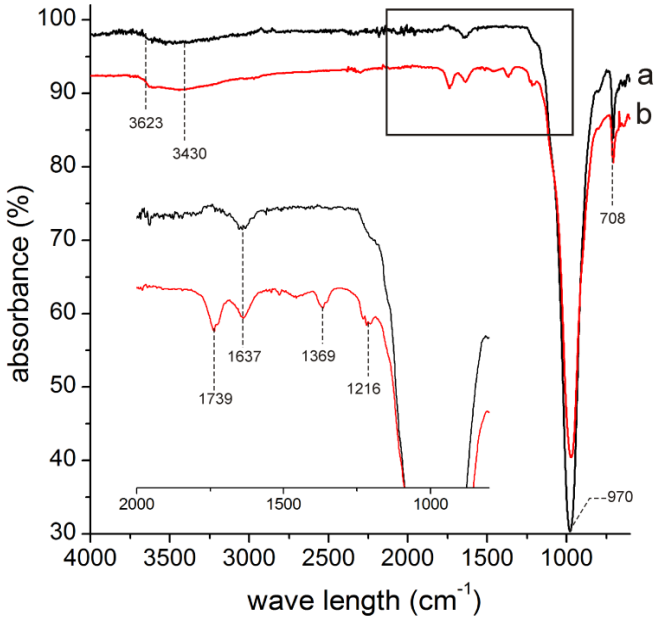

Figure 3.4 FT-IR spectra of (a) K-hect and (b) O-hect.

A solid state ^{13}C NMR spectrum (Fig. 3.5) of O-hect was obtained with clear signals shown at 174 ppm and 45 ppm which is assigned to the carbonyl groups (carbon atoms of C=O) and $N(CH_3)_2$ group of DMAEMA, respectively. Furthermore, the signal at 24 ppm is assigned to the $(CH_3)_2$ group of the bromine ester and the CH_3 group of the polymer backbone. The broad signal at 56 ppm corresponds to CH_2 in the polymer backbone while the signals at 63-69 ppm are assigned to (CH_2CH_2) in DMAEMA and BIEM, confirming the presence of MI on the mica-like surface.

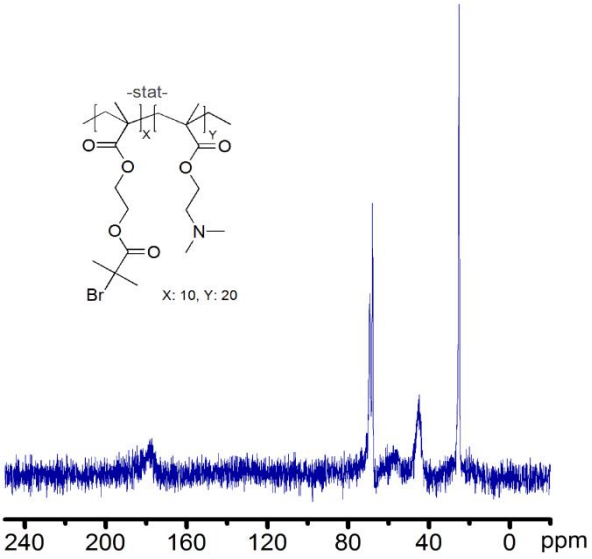

Figure 3.5 ^{13}C solid state NMR spectrum of O-hect.

These qualitative analyses confirmed the presence of MI on the surface of the clay while surface potential measurements combined with TGA provide quantitative analyses of the organic content of the modified platelets. Therefore, we can determine the amount of surface-attached MI at pH=6.8 to be 3.1 wt%. Based on a surface area of 68 m²/g of K-hect we can calculate a grafting density of 0.3 ATRP initiator functions per nm² using the following formula:

$$\rho = \frac{M_I \times N_A}{SA} \qquad (1)$$

Where; ρ is the grafting density (initiator per nm^2), M_I is the molar amount of the initiating species per g of O-hect, N_A is the Avogadro constant and SA is the surface area in m^2/g.

3.1.3 Surface-initiated ATRP of MMA

In addition to the surface bound MI, EBiB was used as a sacrificial initiator due to its structural similarity to the incorporated BIEM in the MI. It has already been shown that surface initiated polymers and polymers grown in solution have comparable molecular weights and polydispersity indices[67, 68]. The use of sacrificial initiator is a facile strategy to determine the chain length of polymers that were grafted from the

clay surface. The ATRP technique allows for preparation of polymers with narrow molecular weight distributions and precise control over the architecture. Table 3.1 gives the number and weight average molecular weights M_n and M_w, respectively, of the free PMMA grown in solution determined by SEC as a function of reaction time. The differences between theoretical and experimental values can be attributed to an initiation efficiency of less than 100%.

Table 3.1 Molecular weights of the free PMMA chains as a function of polymerization time in THF [MMA] : [PMDETA] : [EBiB/MI] : [Cu(I)Cl] : [Cu(II)Cl_2] (3000 : 2 : 0.2/0.8 : 1.2 : 0.3)

Reaction time (min)	Conv.[a] (%)	DP [a]	M_n [a] (kg/mol)	DP [b]	M_n [b] (kg/mol)	M_w [b] (kg/mol)	PDI [b]
10	1	36	3.5	84	8.4	10.0	1.2
20	2	72	7.2	100	10.0	13.0	1.3
30	4	120	12.0	150	15.0	17.0	1.1
60	5	143	14.3	190	19.0	23.0	1.2
120	7	203	20.3	310	31.0	36.0	1.2
300	9	263	26.3	380	38.0	50.0	1.3

[a] determined by ^{1}H NMR spectroscopy. [b] determined by SEC with THF as eluent and PMMA standard calibration.

The reaction shows a controlled character with a very good polydispersity index. Fig. 3.6 (left) shows first-order kinetic of ln[M_0]/[M] as a function of time, whereas, polymerization rate slowed down after 120 min. This indicates that the number of the initiating species remained approximately constant up to 120 min reaction time and then started to decrease. Furthermore, by plotting the molecular weight versus conversion as in Fig. 3.6 (right), a linear increase ascertained the controlled behaviour of the reaction. Based on a surface area of 68 m²/g of K-hect we can calculate a grafting density of 0.08 chains per nm² using the following formula:

$$\rho = \frac{M_p \times N_A}{SA} \qquad (2)$$

Where ρ is the grafting density (chains per nm^2), M_P is the molar amount of PMMA chains with a DP of 380, N_A is the Avogadro constant and SA is the surface area in m^2/g.

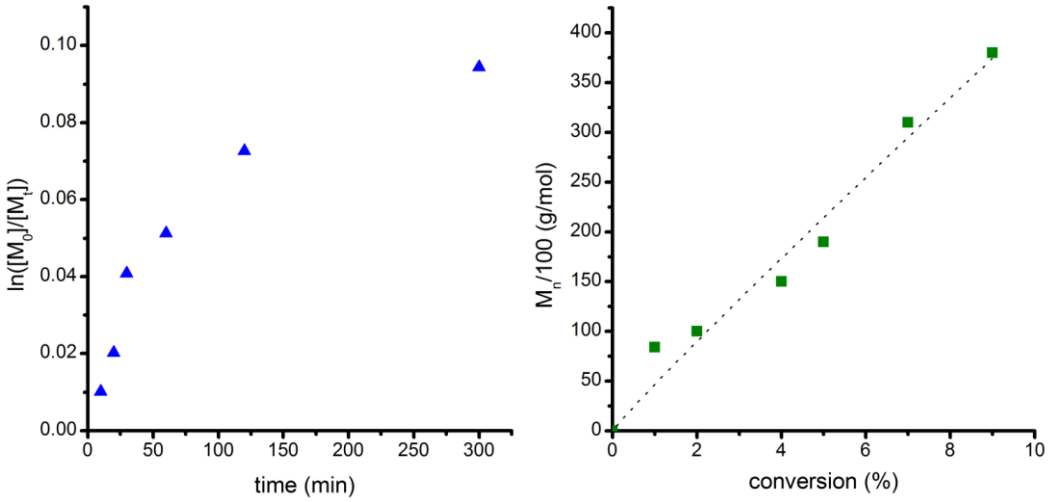

Figure 3.6 (▲) First-order kinetic plot for the polymerization of PMMA. (■) Evolution of the molecular weight with conversion of PMMA.

For a qualitative analysis of the grafted polymer hybrid, FT-IR spectra of neat PMMA and hybrid nanofiller with grafted PMMA chains are compared in Fig. 3.7. Characteristic CH vibrations (2800-3000 cm^{-1}), C=O vibration (1727 cm^{-1}) and C-O vibration (1263 cm^{-1}) confirm the presence of PMMA on the surface even after extensive washing with THF.

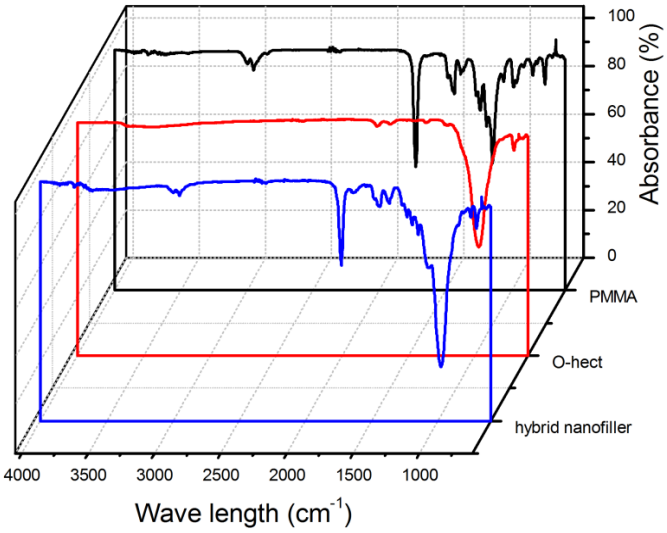

Figure 3.7 FT-IR spectra of neat PMMA (black), surface modified O-hect (red) and hybrid nanofiller (blue).

The amount of surface grafted PMMA was examined by TGA (Fig. 3.8). As expected, nanocomposites with longer polymer chains showed a higher weight loss of organic material. O-hect was found to have 3.1 % loss of volatile materials after heating up to 400 °C (the weight loss prior to 100 °C is neglected due to the traces of solvent). The grafted hybrids showed a weight loss of 15.2 % and 32.4 % for grafted PMMA chains with a DP of 150 and 380, respectively.

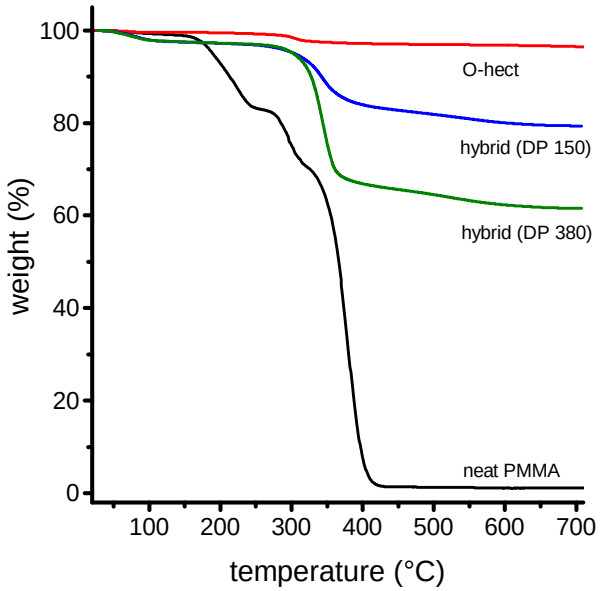

Figure 3.8 TGA measurements showing weight loss versus temperature for O-hect (red), hybrid with PMMA DP 150 (blue), hybrid with PMMA DP 380 (green) and neat PMMA (black).

Powder X-ray diffraction (PXRD) was used to track any changes in the interlamellar spacing during preparation of the hybrid nanofiller. The PXRD patterns of exfoliated K-hect and the hybrid nanofiller are shown in Fig. 3.9.

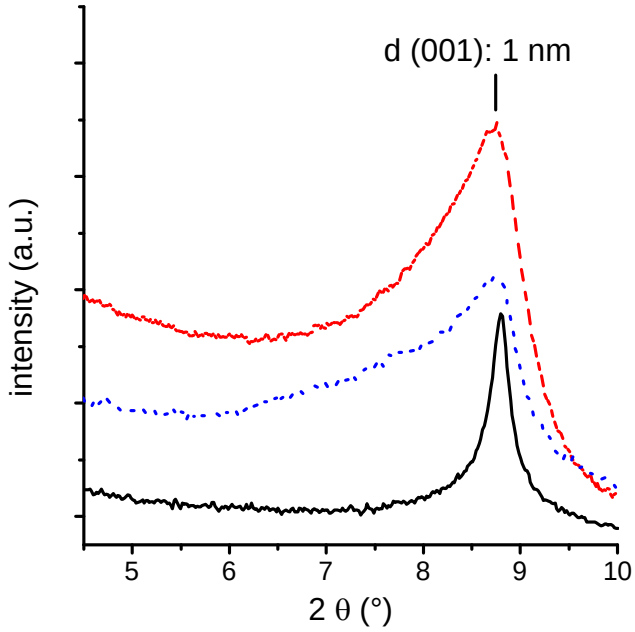

Figure 3.9 PXRD patterns of the (001) peak of K-hect (–), C12-hect (···) and of hybrid nanofiller (DP 380) (---).

The recorded PXRD patterns showed no shifting of the characteristic (*001*) sharp reflection at d_{001}= 9.9 Å which is typical for non-hydrated mica-like clay. This observation assures that all treatments including surface grafting do not have any influence on the interlamellar structure. The morphological changes of the clay's external surface were analyzed using scanning electron microscopy (SEM). In Fig. 3.10 a) a high aspect ratio of K-hect can be seen after exfoliation, having a large lateral extension and smooth surface. In comparison to O-hect (Fig. 3.10 b), the surface grafted hybrid nanofiller has a rougher and coarse surface (Fig. 3.10 c). The pattern is typical for collapsed PMMA chains in a dried state forming mushroom-like structures, as expected for the achieved grafting density.

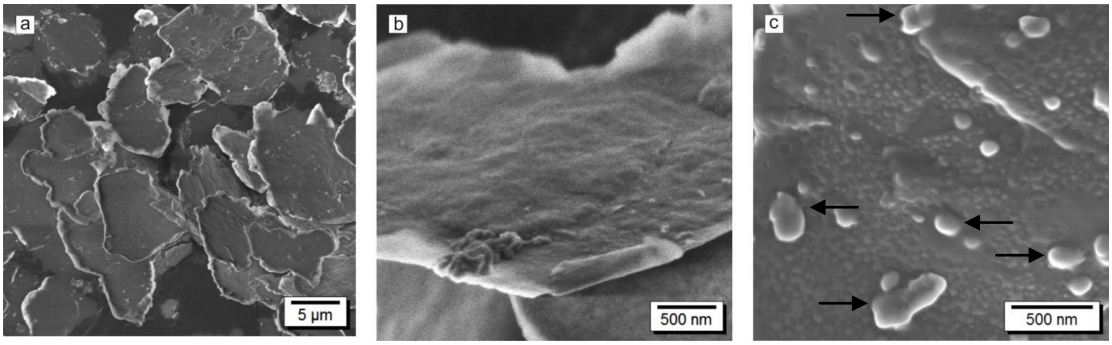

Figure 3.10 SEM images of a) exfoliated K-hect, b) surface morphology prior of O-hect c) Surface of hybrid nanofiller covered with collapsed polymer chains above entanglement length. *(Arrows indicate clay fragments from milling treatment, actual polymers are the smaller structures on the surface).

3.2 Mechanical properties of the clay/PMMA nanocomposites

The mechanical properties of neat PMMA and PMMA/clay nanocomposites determined by tensile evaluation tests at a 5 wt% clay loading are presented in Fig.6. With incorporation of hybrid clay particles the tensile modulus of PMMA/clay nanocomposites showed a significant enhancement compared to neat PMMA. The improvement for C12-hect is already 45 % and hybrid-hect (DP 380) almost doubled the tensile modulus with an improvement of 84 %. The addition of the nanoplatelets has no significant influence on the tensile strength. The elongation at break is reduced by 35% in case of C12-hect and on the contrary shows an increase of 18% for the hybrid-hect (DP 380).

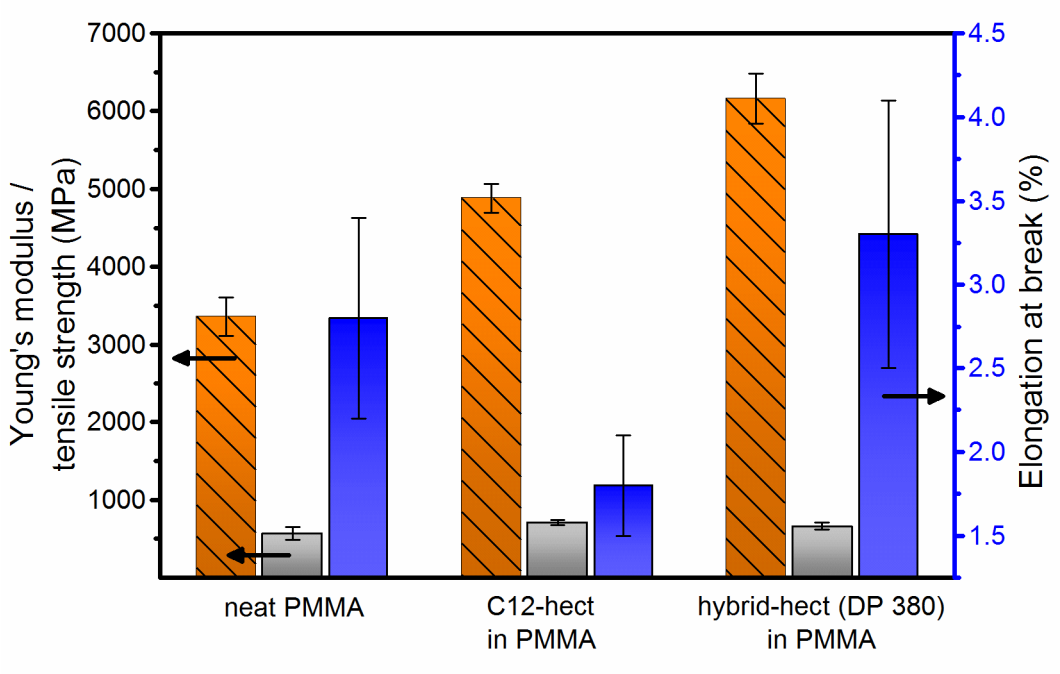

Figure 3.9 Young's modulus (orange, striped), tensile strength (grey) and elongation at break (blue) of neat PMMA and two different clay/PMMA nanocomposites.

The incorporation of high aspect ratio nanoplatelets into a PMMA matrix already leads to a significant reinforcement effect compared to neat PMMA as demonstrated by Fischer et al. in 2012[69]. The optimization of the preparation method through solution blending eliminates any agglomerates formed in a normal melt blending process, which usually are the cause for a significant reduction in the tensile strength[70]. The absence of such agglomerates reduces any local stress concentration in the matrix and thus the tensile strength of the composite is not affected by the addition of the nanofiller.

Significant shifts in the elongation at break behaviour were observed depending on the type of nanofiller. Usually, the addition of rigid nanofillers to a brittle matrix leads to an increase in modulus at the expense of strength, strain and toughness as embrittlement takes place[71].

This behaviour was observed for the incorporation of C12-hect, which increased the modulus by 45 %, but reduced the elongation at break by 35 %. The clay acts as a barrier and thus restricts the sliding of polymer chains among each other. On the contrary a significant increase in modulus and elongation at break was observed for

the novel hybrid nanofiller, which emphasizes the importance of the addition of polymeric chains matching the polarity of the matrix onto the hybrid's surface. This leads to a better adhesion of the nanofiller to the matrix, which generates an effective stress transfer from the matrix to the nanofiller while still participating in the sliding of polymer chains among each other and consequently leads to a significant increase in both, the modulus and elongation at break without sacrificing tensile strength.

3.3 Conclusion

Surface-initiated ATRP was successfully employed to graft PMMA chains from the external basal planes of a shear-stiff, mica-like K-hect to create novel hybrid nanofiller. The employed synthetic fluorohectorite was characterized by a high aspect ratio and homogeneity of layer charge, while the multiple anchoring groups of the synthesized macroinitiator enabled a strong adhesion to the clay's surface. The kinetic study of si-ATRP of PMMA confirmed a controlled polymerization in a linear variation. Furthermore, grafted polymer chains allow for stable dispersions of the hybrids in various organic solvents. The obtained hybrid nanofiller shows a strong reinforcing effect after being compounded into a PMMA matrix due to the synergistic effect of inherent shear stiffness and huge lateral extension of the clay itself and the optimized interface between the hybrid nanofiller and the matrix through addition of a tailored polymeric shell.

Chapter 4: Patchy hybrid particles based on polymer grafted montmorillonite (MMT)

4.1 Preparation of patchy hybrid particles based on MMT

To compatibilize an immiscible binary polymer blend, a hybrid clay particle with homogeneous shell as used in the last chapter is not perfect. Based on the assumption, that a particle with a binary polymer shell should be drawn towards the interface if placed into a mixture of two immiscible components (polymers in a blend or liquids of different polarity) by the Pickering effect, we created disc-like particles with compartmentalized surface, bearing patches of polymer, each matching one of the components of an immiscible blend (Figure 4.1). We hypothesize, that the fraction of polymer chains with unfavourable interactions would collapse and stay close to the solid surface of the hybrid disc, whereas polymer chains with favourable interaction would protrude into the matrix.

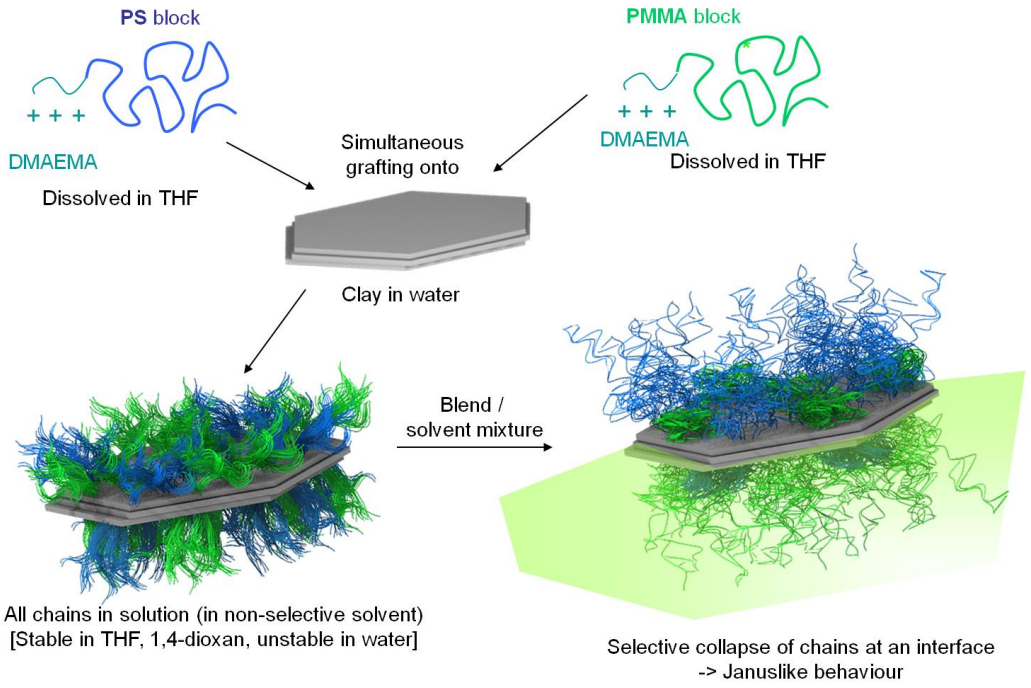

Fig. 4.1 General approach to patchy hybrid nanodiscs *via* grafting of diblock copolymers onto clay surface and selective collapse of chains at an interface.

4.1.1 Synthesis of DMAEMA based diblock copolymers *via* sequential RAFT polymerization

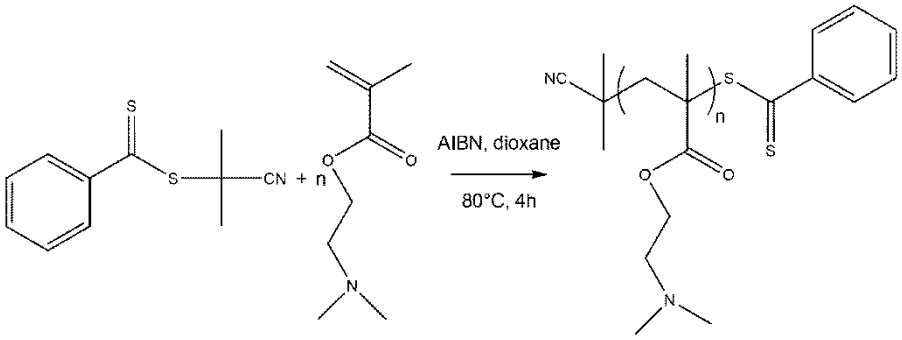

Fig. 4.2 RAFT-polymerization of DMAEMA using 2-cyano-2-propyl benzodithioate (CPBDT) as chain transfer agent

As shown in chapter 3 and in literature, positively charged poly(2-(dimethylamino)ethyl methacrylate) (PDMAEMA) can firmly attach to negatively charged surfaces, like those of layered silicates or colloidal silica[64, 72]. In this chapter, protonated PDMAEMA is incorporated into a diblock copolymer and, as it can be charged positively depending on the pH or permanently by quaternization, is used as a flexible cationic anchoring group to equip clay particles with a polymeric shell. The polymer of DMAEMA is easily accessible *via* RAFT polymerization and can undergo copolymerization with a range of different monomers greatly contributing to the flexibility of modifying clay surfaces with polymers of different polarities, responsiveness and sensitivities. It served as an anchor to the MMT external planes *via* cation exchange. The block-length was kept short and stayed in the range of 14 to 20 repeating units for all diblock-copolymers, as with increasing length of chain it becomes more likely to crosslink several platelets by the same anchoring block.

Controlled radical polymerization by the RAFT-process guarantees low polydispersities of the obtained polymers which is a precondition to generate well defined microphase-seperated solutions and thus control over patch size. Also RAFT polymerization is applicable to various monomers and the synthesis of block-copolymers is facile.

Here, 2-cyano-2-propyl-benzodithioate (CPBDT) was used as RAFT-agent as shown in Fig. 4.2. Typically, the molar ratio of CPBDT : DMAEMA : AIBN was 1 : 10 : 0.3 and the polymerization was carried out until conversion reached 90 %. As shown in Fig. 4.3 the kinetics are of first order with an induction period of several minutes which indicates a fully established RAFT-equilibrium after that time. The molecular weight increases linearly while the PDI is constantly 1.2. The molecular weight is higher than expected from the ratio of CTA to monomer. Analysis of the monomer unit ratios in the final diblock *via* ^{1}H NMR analysis confirmed the M_n values of the precursors obtained from SEC (Dimethylacetamid (DMAc) as eluent and PDMAEMA standard calibration, Fig. 4.3). This observation can be explained by a low transfer constant of the initial CTA molecule, resulting in nearly free radical polymerization kinetics until the CTA has added a monomer unit, increasing its transfer constant and thus enabling controlled polymerization. This is known as the hybrid effect and in this case results in an effective ratio of CTA to monomer of about 1 to 15 and explains the elevated molecular weights. As the targeted degree of polymerization is very low the molecular weight evolution is very sensitive to the amount of CTA effectively participating in the RAFT-process. Nevertheless the variation of 5 Units of DMAEMA was accepted, as it is not expected to influence the properties of the final hybrids in a substantial way[72].

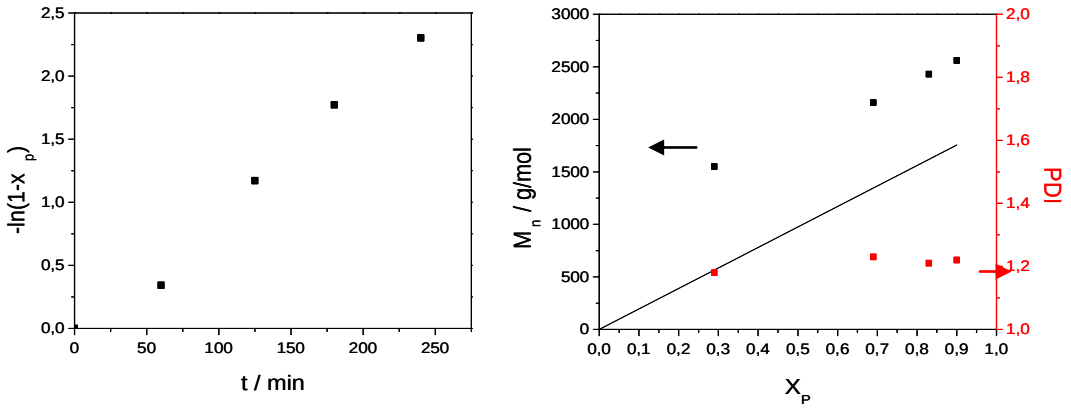

Fig. 4.3 First-order kinetics of the RAFT polymerization of DMAEMA with CPBDT in 1,4-dioxane at 80 °C (left). Evolution of the molecular weight and PDI (right). The theoretical molecular weight is given as a straight black line. Determined with DMAc as eluent and PDMAEMA standard calibration

In this chapter, we copolymerized PDMAEMA with polystyrene (PS) and poly(methyl methacrylate) (PMMA) in a block-like fashion to achieve maximum compatibility with both phases of a PS/PMMA binary blend. To synthesize the diblock copolymers PDMAEMA macro-CTAs were transferred to a degassed solution of the second monomer directly without any purification. This procedure delivers the diblock copolymers in the most facile and straightforward way. As the second monomer was applied in a 100- to 500-fold excess and the polymerization of the precursor was carried out up to high conversions the amount of unconsumed DMAEMA in the second block is negligible. Table 2 shows the basic information about the synthesized diblock-copolymers.

Table 2 Molecular weight of the PDMAEMA-macro-CTA, the diblock-copolymers as well as the conversion of the second monomer and the final PDI.

Formula [a]	$M_n^{\text{macro-CTA}}$ / kg/mol [b]	M_n^{total} / g/mol [b]	$X_p^{\text{second block}}$ / % [c]	**PDI** [b]
D_{17}-*b*-M_{300}	2.9	33.0	64	1.1
D_{16}-*b*-S_{360}	2.6	39.0	50	1.3

[a] repeating units of DMAEMA calculated by subtracting the molecular weight of CPBDT (221.0 g/mol) and dividing by the molecular weight of DMAEMA (157.2 g/mol), repeating units of the second block calculated by subtracting the molecular weight of DMAEMA block and dividing by the molecular weight of the respective monomer, acronyms: D: DMAEMA, S: styrene, M: MMA; [b] determined by SEC with DMAc as eluent and PS and PMMA standard calibration, respectively; the PDI of all macroCTAs was well below 1.3; [c] calculated from ^{1}H-NMR by integration of the decreasing vinyl groups against peaks of the internal standard, 1,3,5-trioxane.

In Fig. 4.4 the SEC-traces of D_{17}-*b*-M_{300} and D_{16}-*b*-S_{360} are shown. It can be seen that the DMAEMA precursor is completely consumed with time indicating a quantitative blocking efficiency. Nevertheless, in the progress of the polymerization a shoulder at lower molecular weights is formed. This could be due to irreversible termination *via* disproportionation or introduction of oxygen during sample extraction (for SEC and NMR).

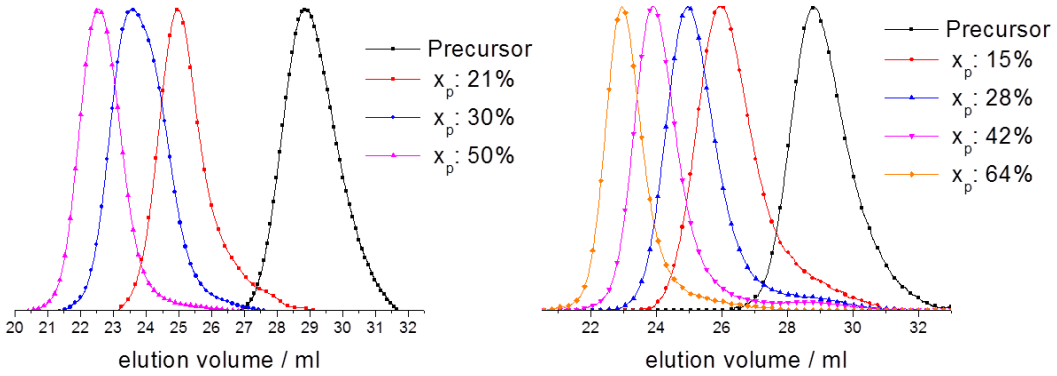

Fig. 4.4 Evolution of SEC-traces of D_{17}-*b*-S_{360} (left) and D_{17}-*b*-M_{300} (right) with conversion.

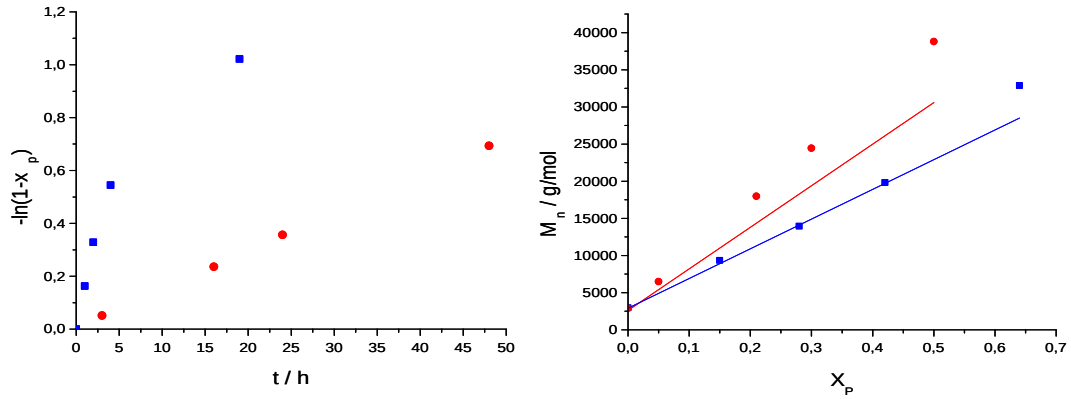

Fig. 4.5 First-order kinetics of the RAFT polymerization of MMA (blue squares) and PS (red circles), respectively, with PDMAEMA-Macro-CTA in 1,4-dioxane at 80 °C (left). Evolution of the molecular weights of D_{17}-*b*-M_{300} (blue squares) and D_{16}-*b*-S_{360} (red circles), respectively (right). Theoretical molecular weights are given in straight lines with respective color. DMAc was used as eluent and PS and PMMA as respective standard calibration

For the styrene containing diblock copolymers polymerization was slower than for methacrylate based monomers (Fig. 4.5 left). This rate retarding effect was only observed for this monomer and is discussed in literature as originating either from terminating side reactions of the intermediate radicals or extremely slow fragmentation of those species.[73]

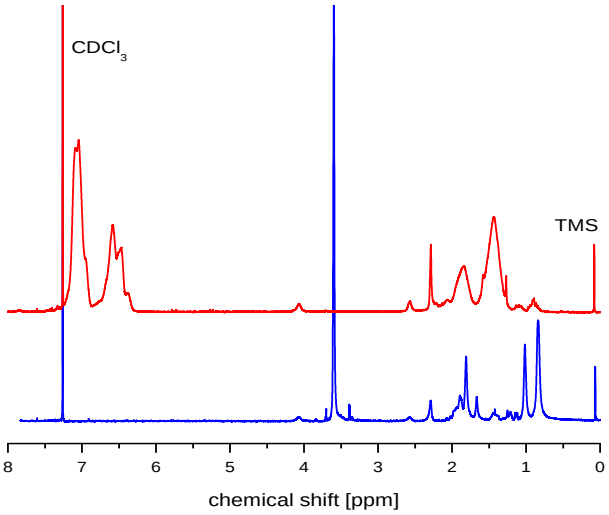

Fig. 4.6 ^{1}H-NMR spectra of D_{17}-*b*-M_{300} (blue) and D_{16}-*b*-S_{360} (red).

The final compositions were determined as $PDMAEMA_{16}$-b-PS_{360} and $PDMAEMA_{17}$-b-$PMMA_{300}$ by the ^{1}H NMR (Fig. 4.6) integral ratios between characteristic signals of the respective two blocks (PS: 5H, aromatic, δ 6.8-7.3 ppm; PMMA: 3H, $-CH_3$, δ 3.6 ppm; PDMAEMA: 2H, $-CH_2-$, δ 4.1 ppm).

4.1.2 Solution behaviour of the diblock copolymers

MMT is best dispersed in water and does not disperse in organic solvents. As a consequence, modification of the basal planes has to take place in water if high degrees of exfoliation for minimum stack heights and maximum surface area are desired. The diblock copolymers used for surface modification consist of a hydrophilic, charged DMAEMA block and a hydrophobic PS or PMMA block. Both blocks are completely soluble in THF, but the hydrophobic block is insoluble in water. A diblock copolymer solution in THF will form micelles upon contact with water, where the PS or PMMA block will form the inner core and the charged DMAEMA parts make up the hydrophilic shell. There are two routes to form micelles: Either, slow addition of water to a solution of polymer in THF, creating near-equilibrium state micelles, or rapid addition of the THF solution to a large quantity of water, creating smaller micelles, freezing them in a non-equilibrium state. A control over micelle size is desired, as we consider a strong relation between micelle sizes and

patch size on the surface of the clay after modification. An optimum grafting onto process and development of patches is expected if the diblock-copolymer micelles are clearly smaller than the MMT clay, which has an average diameter of 300 nm, determined by SLS and TEM. Otherwise attachment of different platelets to the same micelle can lead to aggregation and coverage with only one polymer species becomes more likely. The micelles of D_{17}-*b*-M_{300} and D_{16}-*b*-S_{360} were investigated by DLS and TEM. Therefore the polymers were dissolved in THF (5 mg/ml) and after filtration into a sample vial filtered water (pH=6.5) was added dropwise until the amount of water was 10 % (Fig. 4.7 a, dotted line) and 15 % (Fig. 4.7 a, compact line) of the volume, respectively.

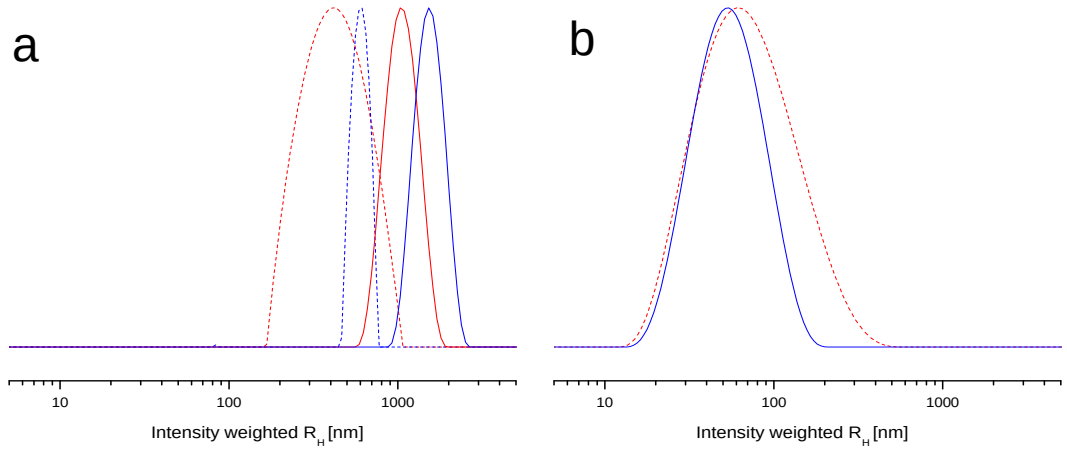

Fig. 4.7 Dynamic light scattering of D_{17}-*b*-M_{300} (blue line) and D_{16}-*b*-S_{360} (red line) a) in 1/1 (V/V) THF/water solutions prepared by addition of water to a solution in THF, 10 % water dotted line, 15 % water compact line, b) in 1/1 (V/V) THF/water solutions prepared by rapid addition of THF polymer solution into stirred water.

The dynamic light scattering results are shown in Fig. 4.7 a). The volume fraction of the hydrophilic PDMAEMA block of both polymers, D_{17}-*b*-M_{300} and D_{16}-*b*-S_{360}, is less than 30%, which lead to the formation of vesicles well above the size of the MMT with z-average hydrodynamic radii of 670 nm for D_{17}-*b*-M_{300} and 410 nm for D_{16}-*b*-S_{360} (Fig. 4.7 a). From the light scattering experiments it is obvious that attempted control of micellication of the synthesized polymers by equilibration even at a low

volume ratio of water to THF of 10% will lead to structures, which are considered to be too large for useful modification. Nevertheless, rapid addition of 1 mg/ml polymer solutions from THF into a vial with the same volume of stirred, filtered water (pH=6.5) resulted in very small micelles of sizes below 100 nm, with z-average radii of 67 nm, and 50 nm respectively (Fig. 4.7 b).

4.1.3 Modification of the basal planes

In all experiments, which showed successful modification, polymers (30 mg, 1 mg/ml) were simply dissolved in THF and added directly to a rapidly stirred clay suspension in water (100 mg, 5 mg/ml, pH=6.5) *via* a small cannula, without formation of micelles prior to addition.

Concentration of polymer in THF was kept low and the charged PDMAEMA block is held responsible to prevent precipitation upon contact with the water phase and instead form small (below 100 nm) frozen micelles, keeping the polymer reactive enough for surface modification to take place, similar to the experiment described above (Fig 4.7 b). The assumed micellar sizes are in good agreement with patch sizes observed in SEM (12 - 45 nm, median: 23 nm, 60 individual patches taken into account) (Fig. 4.8 left).

Upon addition of polymer solution and stirring for several minutes, flocculation occurred and after a short time of standing still all of the once stable suspension sedimented, leaving a clear supernatant. After repeated centrifugation and washing with THF the unattached polymer was removed and the micelles sitting on the clay's surface were broken up. Therefore a morphology change from micelle to lamella had to occur by THF lowering the T_g of the hydrophobic block below room temperature, rendering it flexible again and exposing it to the solvent. Afterwards the hybrid formed a stable suspension in THF, which is a clear sign for successful organophilization.

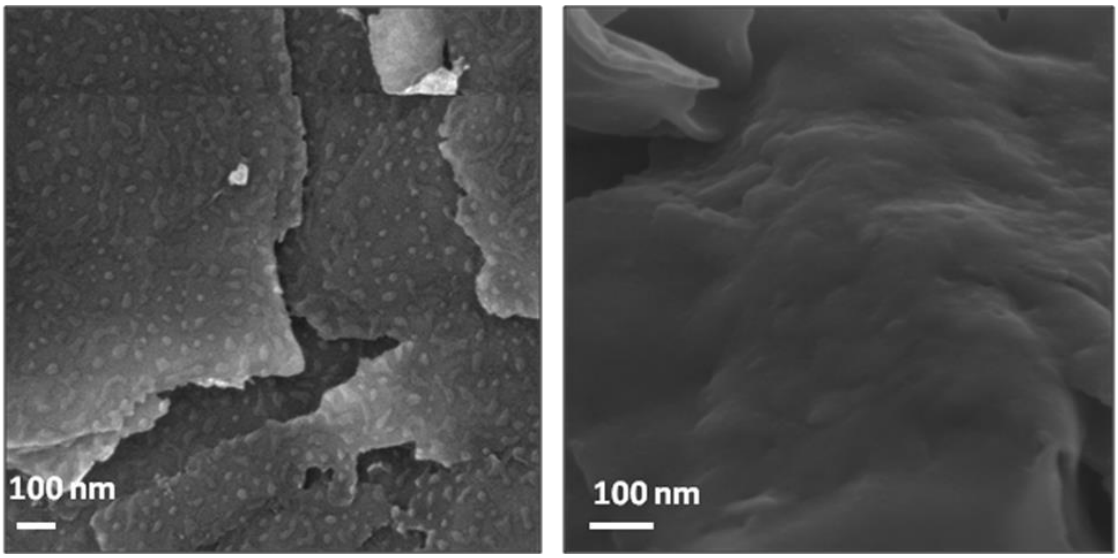

Fig. 4.8 SEM images of hybrids based on hectorite (left) and MMT (right) modified with a 1:1 (molar) mixture of D_{17}-*b*-M_{300} and D_{16}-*b*-S_{360} in THF

By this approach it was possible to modify several types of clay (for kaolinite see chapter 5): The small particle (tactoid) size and agglomeration into band-like structures or self-supporting clay films upon drying makes it difficult to visualize the successful grafting and its patchiness in general on the surface of MMT. Since no individual platelets are visible, but rather agglomerates of several µm in diameter, it is impossible to distinguish polymer from platelets. As a proof of principle larger and stiffer synthetic clay was used. The same shear-stiff K-fluorohectorite from chapter 3 was modified *via* "grafting onto". Qualitative analysis of SEM images showed less grafting density and more inhomogeneous surface coverage (Fig. 4.8) as compared to experiments with polymeric shells attached *via* a "grafting from" technique (Fig. 3.10).

While SEM analysis of the synthetic clays delivered evidence for successful grafting of polymer onto the clay surface, it was not possible to prove grafting of *both* polymer species in this way. ^{1}H-NMR analysis was used to determine whether preferential adsorption of either of the polymers occurred. Ratios between peaks of the 5 aromatic protons in the PS block (δ=6.4-7.2 ppm) and the 3 protons of the CH_3-O- ester group of the PMMA block (δ=3.6 ppm) where compared, between the solution used to modify the clay and the supernatant after centrifugation for the first

time. Both ratios of PS to PMMA were roughly the same before and after modification (deviation of less than 10%), which leads to the assumption that adsorption is primarily controlled by the PDMAEMA block, which is of comparable length in all cases, and there is no significant preferential adsorption depending on the species of the second block with the given species.

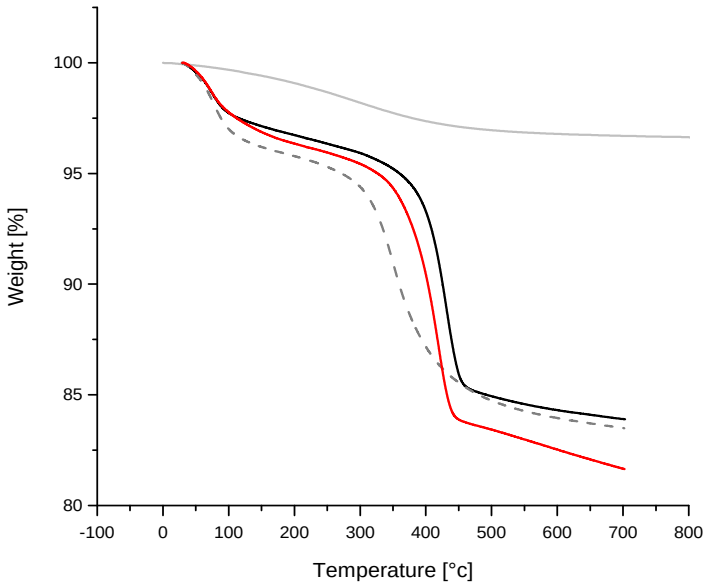

Fig. 4.9 TGA results showing the temperature dependent weights of different hybrid particles: unmodified MMT (solid gray), D_{16}-*b*-S_{360} modified MMT (solid black), D_{17}-*b*-M_{300} modified MMT (striped gray), patchy hybrid MMT modified with both aforementioned diblock copolymers (solid red)

To quantify the amount of surface-bound polymer a thermogravimetric analysis (TGA) was performed (Fig. 4.9): unmodified MMT showed a total mass loss of 2 %, while all hybrids showed a mass loss of around 12-15 % in the most relevant region (200-500 °C), which gives a calculated grafting density of 0.5 units of DMAEMA per nm² for completely exfoliated MMT using the following formula:

$$\rho = \frac{M_D \times N_A}{SA} \qquad (1)$$

Where; ρ is the grafting density (initiator per nm^2), M_D is the average molar amount of DMAEMA units per g of hybrid, N_A is the Avogadro constant and SA is the surface

area of 68 m^2/g. The calculated value is around half of the cation exchange capacity (CEC) value provided by the company for the employed MMT (PGV) in a theoretical delaminated state and. The discrepancy can be explained by incomplete exfoliation.

4.2 Mechanical properties of the clay/PMMA/PS nanocomposites

4.2.1 Preparation of clay/PS/PMMA blends

Dually modified PS/PMMA-patchy hybrid particles, with the polymer patches on each side should be able to selectively collapse or extend to match the surface tension of the polymer phase they reside in, were tested as compatibilizers in films of PS/PMMA blends cast from THF, a good solvent for both polymers and a good dispersant for the hybrids. Located at an interface, each side should collapse the incompatible polymer chains and extend the compatible ones into the matrix, forming a Janus-like structure.

For comparison and to be able to estimate the effect of the patchy character additional blends with homogeneously modified clay (either PS or PMMA as shell) and blends with unmodified MMT were prepared by solvent casting under the same conditions. A PS/PMMA ratio of 1:2 (wt/wt) was chosen. The Flory-Huggins parameter for a blend of this molecular weight is χ_{SM} = 0.041 at 20 °C[74] indicating its incompatibility.

The samples for transmission electron microscopy (TEM) were prepared by casting the polymer solution with dispersed clay into a glass vial followed by slow drying and microtome cutting. The difference between PS and PMMA is clearly visible in the TEM images (Fig. 4.9) even without selective staining. Dark grey areas result from stronger electron contrast of PS and light grey areas from PMMA, which is more easily damaged by the electron beam. The clay particles appear even darker, almost black, and their profile shapes are clearly visible due to their strong contrast, the completely white regions are holes in the film introduced during ultra microtome cutting.

We are aware of the fact that solvent evaporation will trap the system in a metastable state and such prepared films can only show a qualitative aspect of compatibilization achieved by our hybrid particles. For pure PS/PMMA blend films of comparable molecular weight without compatibilizer, it is known, that large (several µm in diameter) spherical domains of the minority phase inside a matrix formed by the majority phase result from phase segregation[51]. From literature on classical organoclays (e.g. Cloisite 20A), it is known, that modification with simple alkyl chains will lead to dispersion only in the PMMA phase of a PS/PMMA blend and formation of clusters in PS homopolymer blends.[75] Analysis of blends mixed with PS-grafted MMT (modified with D_{16}-*b*-S_{360}) showed that the hybrids without exception stay in the PS phase or assemble at the interface, though no strong tendency for interfacial interaction is observed (Fig. 4.10 a). Similar results are obtained for hybrids based on PMMA-grafted MMT (modified with D_{17}-*b*-M_{300}). Both hybrids stay in the phase of the polymer their surface is modified with. Though being the minority phase, we can find prominently huge domains of PMMA, filled with randomly oriented hybrid platelets (Fig. 4.10 b). The observed polygonal shape of polymer domains can be attributed to increased viscosity of the filler-rich phase rather than interfacial activity, as there are only a few platelets directly assembled at the interface.

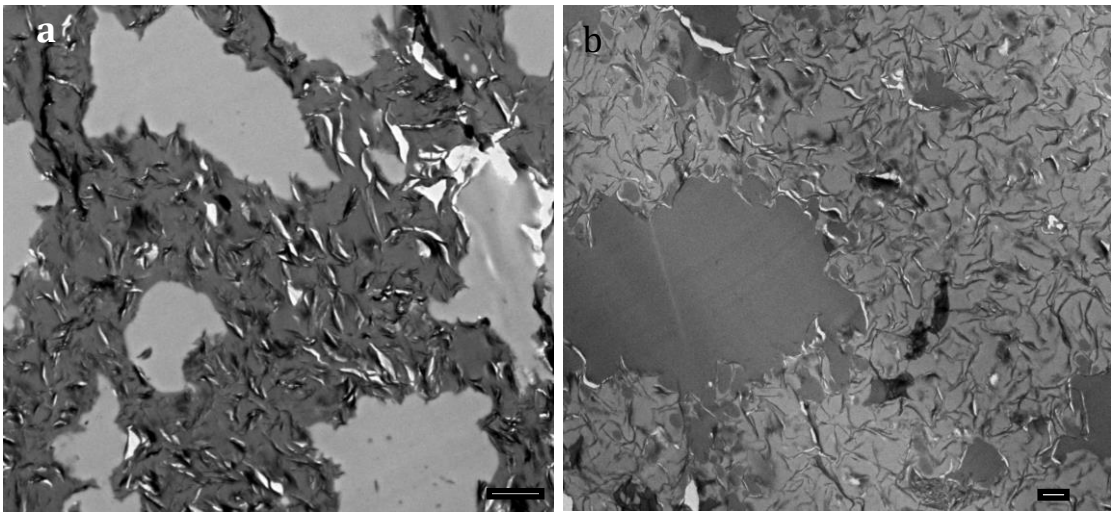

Fig. 4.10 TEM images of 2:1 (wt/wt) PS/PMMA blend films a) showing D_{16}-*b*-S_{360} modified hybrids in the PS phase only, b) D_{17}-*b*-M_{300} modified hybrids in PMMA phase. The fraction of the added hybrid is 5 wt% and the scale bar represents 1 µm.

Blends compatibilized with patchy hybrid particles (shell based on modification with a 1:1 (molar) mixture of D_{16}-*b*-S_{360} and D_{17}-*b*-M_{300}) show a completely different structure. Hybrids are randomly oriented and distributed over the whole blend in both phases and the interface (Fig. 4.11 a). The domain size is reduced compared to blends compatibilized with unmodified and single-polymer-species modified clay. Domain shapes are completely irregular (Fig. 4.11 b), following the shape of platelets where they reside in the interface. As not all of the interfacial area is covered, the hybrids act as a physical barrier and increase viscosity, preventing the formation of large spherical domains (Fig. 4.11 b). Regarding the structure of the polymeric shell of the patchy hybrids, we expect three different cases: a hybrid residing in the PS phase will have its PMMA chains collapsed near the clay surface, screened by extended PS chains, interacting with the matrix. Hybrids in the PMMA phase will show opposite behaviour, where PMMA chains are extended and PS chains are collapsed. In an interface, a hybrid would show both aforementioned behaviours at once, according to the polymer phase the respective side is facing.

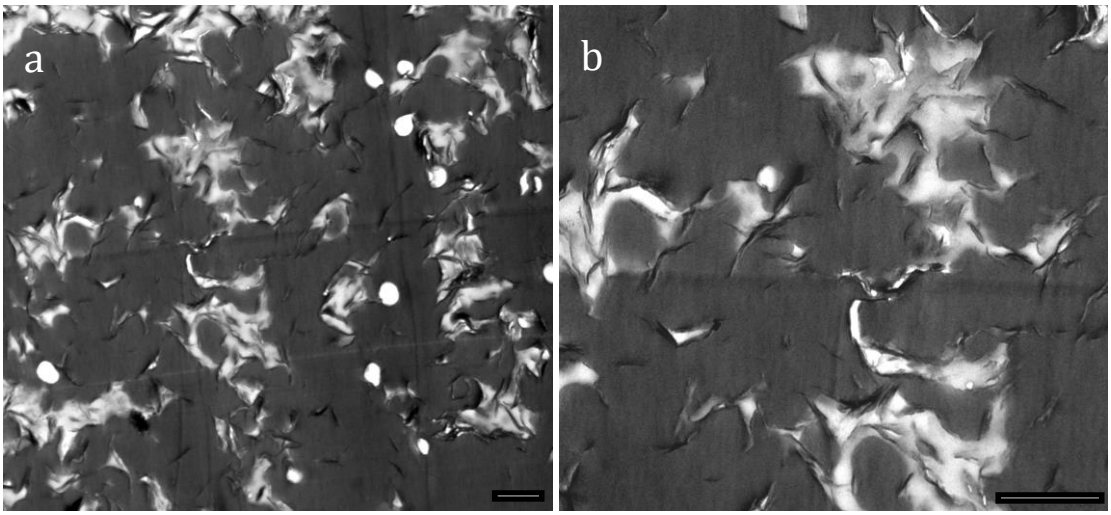

Fig. 4.11 TEM images of 2:1 (wt/wt) PS/PMMA blend films a) showing patchy hybrids with PMMA and PS shell in the PS phase, the PMMA phase and the interface, b) close up. The fraction of the added patchy hybrids is 5 wt% and the scale bar represents 1 µm.

As the blend morphology is created under influence of THF as a solvent and is fixated only after slow evaporation of the solvent, the shell of each hybrid has enough time

and is flexible enough to extend and collapse its polymer chains to match the interfacial tension / surface energy of the polymer phase it resides in. Compared to a pure Janus or Pickering particle it can find its energetic minimum not only at an interface, but inside one of the phases as well.

4.2.2 DMA of the blends

From the variety of DMA data, the storage modulus, E', is plotted in dependence of the heating temperature, T. (Fig. 4.12).

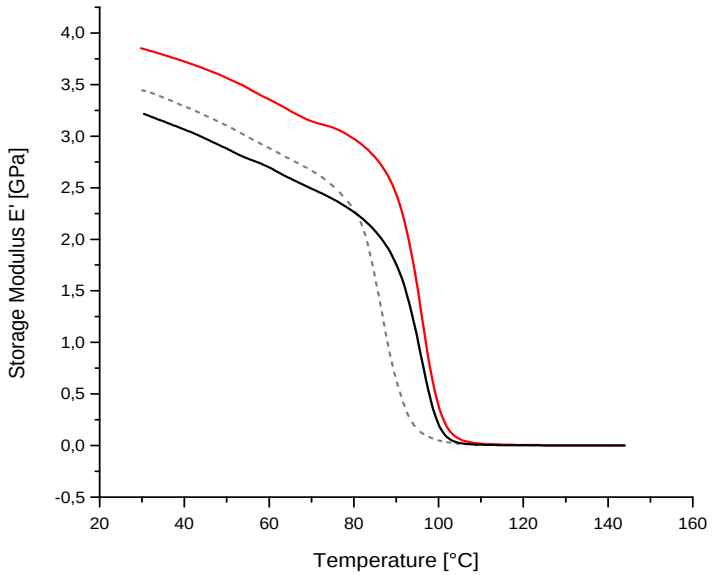

Fig. 4.12 DMA results showing the temperature dependend storage moduli of 2:1 PS:PMMA blends: uncompatibilized pure blend (solid black), blend compatibilized with 5 wt% alkylammonium-modified PGV (dotted gray) and compatibilized with patchy hybrids of PGV (solid red).

The storage modulus of a pure, uncompatibilized 2:1 PS/PMMA blend is 3.2 ±0.1 GPa at 35 °C, compatibilization with a C12-alkylammonium modified MMT resulted in a storage modulus increase of ~7 % to 3.4 ±0.1 GPa, while compatibilization by a patchy hybrid resulted in an increase of 17 % to 3.9 ± 0.1 GPa (Fig. 4.12). Thus, a significantly higher degree of reinforcement is observed by compatibilizing the blend with patchy hybrids than with simple organoclay.

4.3 Conclusion

The experimental data presented confirm the successful grafting of different patches of two diblock copolymer species onto the surface of clays from the smectite group, creating novel patchy hybrid particles. We used a versatile and simple approach to synthesize functional diblock copolymers which consist of a short anchoring block to attach to the clay surface and a longer block adding the desired polarity or functionality. A combination of two or more of different diblock copolymers grafted onto clay can lead to a dynamic shell which is able to adapt to environments of different polarity and even show interfacial activity in immiscible polymer blends. The dispersion in both phases and the interface of an immiscible polymer blend indicates the relevance of the theoretical concept of selective polymer chain collapse and extension in the polymeric shell of the particles and leads to a reinforcing effect, shown in an increase of up to 17 % in Young's-modulus.

While the presented method did not lead to Janus-type behaviour, characterized by preferable presence in the interface, the method should allow further interesting combinations of different diblock copolymers to functionalize the patchy shell of the hybrid particles, opening up new fields unreachable with homogeneously modified particles.

Chapter 5: Hybrid Janus particles based on polymer modified kaolinite

This chapter is the result of the cooperation with Dunja Hirseman and major parts of this chapter were published in Polymer 2013, 54, 1388-1396 under the title: “Hybrid Janus particles based on polymer-modified kaolinite” by Stephan Weiss, Dunja Hirsemann, Bernhard Biersack, Mazen Ziadeh, Axel H.E. Müller, Josef Breu, Text and respective figures are adapted and reprinted with permission. Copyright 2013 Elsevier

5.1 Preparation of hybrid janus particles based on kaolinite

The investigations of randomly compartmentalized, patchy hybrid particles based on MMT showed interfacial activity too low to attach to the interphase between PS and PMMA in an immiscible blend of both. One of the reasons we found was the flexibility of the particle shell, with immiscible patches collapsing and miscible patches extending into the matrix, thus keeping the hybrid particle flexible enough to adapt to its surroundings, independent of where it was located. The next logical step was to create disc-like Janus hybrid particles, with a shell comprised of exactly two chemically distinct, oppositely located compartments, increasing intrinsic polarity of the hybrid and targeting the interphase of the blend as the energetically most favourable location. 2:1 Smectites, like hectorite and montmorillonite are not well suited to create Janus particles, as it is very tedious to selectively address each of their external basal planes individually. However, due to its polar crystal structure, the two opposing external basal planes of kaolinite, TS and OS are truncated by distinct functional groups and may selectively be modified by simple cation exchange and covalent grafting via catechol groups, respectively, making it the perfect base for a disc-like hybrid Janus particle. As an example we chose poly((2-dimethylamino)ethyl methacrylate)-block-polystyrene (D_{16}-b-S_{115}) and poly(3-(2,3-dihydroxy-benzoyloxy)propyl methacrylate)-stat-(methyl methacrylate)) (PCM).

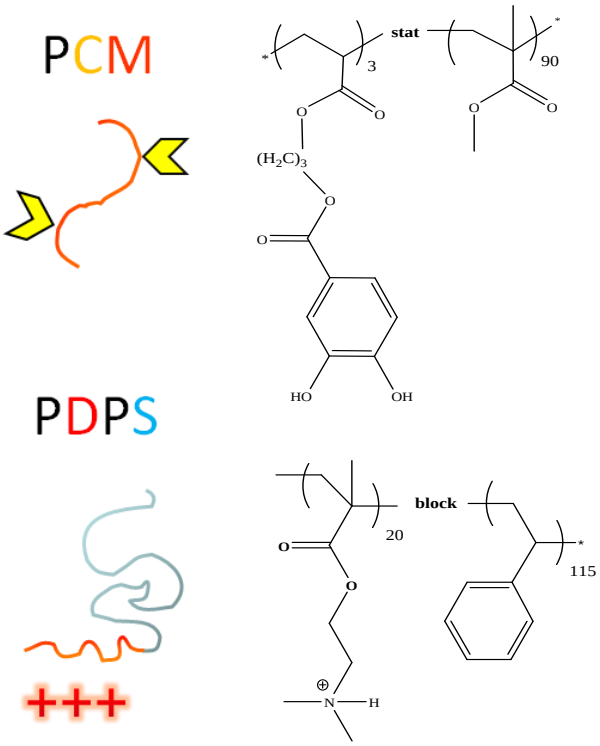

Fig. 5.1 Structure of poly(3-(2,3-dihydroxybenzoyloxy)propyl methacrylate)-stat-(methyl methacrylate) (PCM) (top) and poly(2-(dimethylamino)ethyl methacrylate)-block-polystyrene (D_{16}-*b*-S_{115}) cations (bottom).

PCM is a statistical copolymer, while D_{16}-*b*-S_{115} is a block copolymer (Fig. 5.1). Consequently, both modifiers interact with the kaolinite basal planes in a different manner (Fig. 5.2). PCM will likely be close to the OS, forming short loops or lying flat. In contrast, the polystyrene block might arrange brush-like on the TS of the kaolinite. The resulting Janus particles are tailored for compatibilizing PS-PMMA or industrially more relevant PPE–SAN (poly(2,6-dimethyl-1,4-phenylene ether) (PPE), poly(styrene-*co*-acrylonitrile) (SAN)) blends[50, 51].

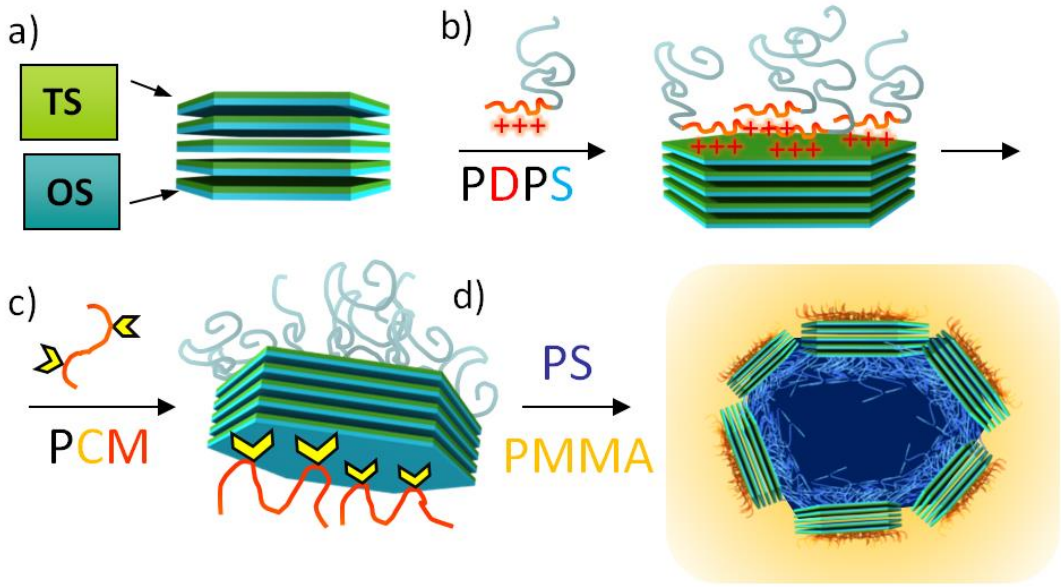

Fig. 5.2 Schematic picture of a) pristine kaolinite, b) modified with D_{16}-*b*-S_{115} on the tetrahedral surface (TS), c) further modified with PCM on the opposite octahedral surface (OS) and d) embedding of the final hybrid particle at the interface in a PS-PMMA blend.

5.1.1 Synthesis of the copolymers PCM and D_{16}-*b*-S_{115}

Synthesis of the catechol-modified poly(methyl methacrylate) copolymer (PCM)

Initially, a suitable catechol modified methacrylate monomer was prepared for copolymerization with methyl methacrylate (MMA). 3,4-Dibenzoxy-(3-hydroxypropyl)benzoate **2** was obtained from 3,4-dibenzoxybenzoic acid **1**.[57] Reaction of **2** with methacryloyl chloride gave the mixed diester **3** (Scheme 5.1).

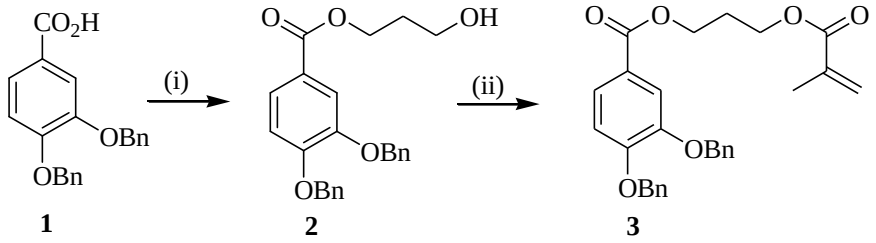

Scheme 5.1 Synthesis of the catechol monomer. Reagents and conditions: (i) $SOCl_2$, $CH_2(CH_2OH)_2$, Et_3N, THF / DCM, r.t., 5 h, 51%; (ii) $CH_2C(CH_3)COCl$, Et_3N, DCM, r.t., 3 h, 67%.

Monomer **3** was copolymerized with a 30-fold excess of MMA by free radical polymerization using AIBN as initiator and dodecanethiol as transfer agent to gain control and reduce molecular weight, giving copolymer **4**. 1H NMR spectroscopy and

integration of the proton signals of the copolymer **4** confirmed the applied ratio of 1:30 of monomer **3** and MMA in the copolymer. Subsequent catalytic hydrogenation removed the benzyl protecting groups from the copolymer **4** giving the catechol modified copolymer **5** (Scheme 5.2). Both FT-IR and 1H NMR spectroscopy gave evidence for the free catechol moieties of the copolymers 5 and revealed new signals for the catechol hydroxy groups of the copolymer (5: vmax = 3392 cm-1; dH = 9.32, 9.81). The synthesized copolymer has a number-average molecular weight Mn = 10,000 g/mol (based on PMMA calibration) with a PDI of 1.7.

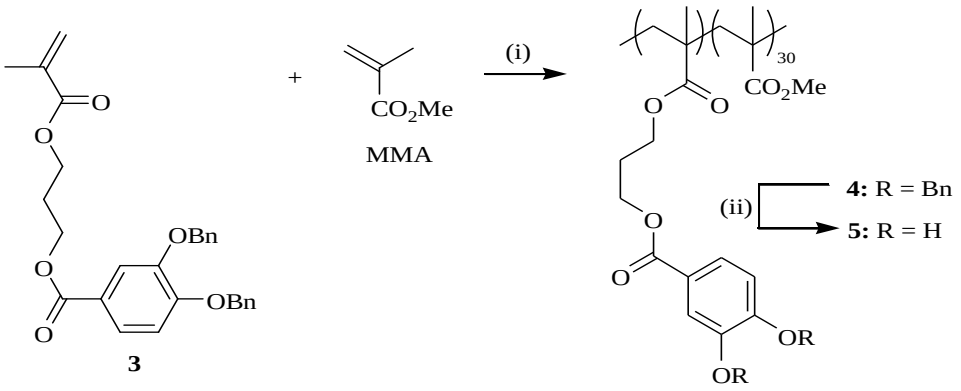

Scheme 5.2 Synthesis of PCM. Reagents and conditions: (i) AIBN, THF, reflux, 5 h; (ii) H_2, Pd/C (10%), MeOH / dioxane, r.t., 5 h.

Synthesis of the PDMAEMA-b-PS block copolymer (PDPS)

The selected block copolymer was synthesized via sequential RAFT polymerization, has a number average molecular weight of 16000 g mol-1 and exhibits a narrow molecular weight distribution with Mw/Mn ~1.13 (determined by DMAc SEC with PS calibration). DMAEMA was polymerized as a first block achieving a conversion near 99 % (as determined by ^{1}H- NMR), an Mw of 3200 g/mol and a PDI of 1.20. This PDMAEMA was utilized as a macro-RAFT agent without further purification and for the polymerization of styrene. The final composition was determined as $PDMAEMA_{20}$-PS_{115} by the ^{1}H-NMR integral ratios between characteristic signals of the two blocks (PS: 5H, aromatic, δ 6.8–7.3 ppm; PDMAEMA: 2H, –CH_2–, δ 4 ppm).

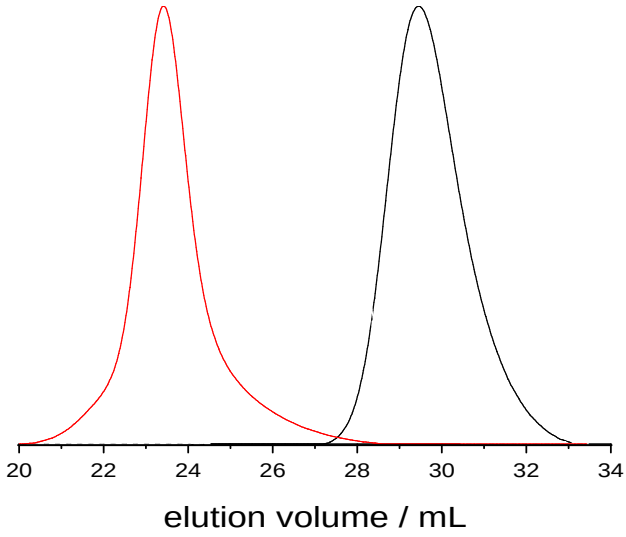

Fig. 5.3 SEC-Traces of Poly(DMAEMA) precursor (black curve, right) and D_{16}-*b*-S_{115} diblock copolymer (red curve, left).

5.1.2 Modification of the kaolinite basal planes

It is possible to modify each side (TS and OS) of the kaolinite specifically and individually[21] without influencing the other side. The chosen order of modification, starting with D_{16}-*b*-S_{115} has a practical purpose, as the DMAEMA block of the D_{16}-*b*-S_{115} is charged at the pH of 6 and thus kaolinite can be modified in aqueous suspension, where it is dispersed best. After that, the one-sidedly modified kaolinite can be dispersed in THF more easily than unmodified kaolinite. PCM is soluble in THF, but not in water. Nevertheless pristine kaolinite can be modified by PCM as a first step as well, but for that it has to be dispersed in THF by vigorous stirring.

Successful surface modification of kaolinite with both polymeric modifiers was proven by ^{13}C solid-state MAS (magic angle spinning) NMR, while TGA (thermogravimetric analysis) was performed to estimate the amount of polymer bound to both external basal surfaces of kaolinite. Moreover, the selective nature of the modification was confirmed indirectly by qualitatively comparing the sedimentation stability (as determined by LUMiFuge®) of suspensions of differently modified samples.

We used a natural fine-grained kaolinite with typical dimensions of the ideally hexagonal platelets that were < 2 µm in diameter and up to 70 nm in height. The specific surface area was approximately 4 m^2 g^{-1}, and about 80 % of this area could be attributed to the external basal surfaces. Nevertheless, the detection of monolayer coverage of the external surfaces required highly sensitive analytical methods, and the proof of the selective modification is inherently difficult, but selectivity of anchoring groups was already shown in our previous publication[21].

^{13}C solid-state NMR spectra of kaolinite samples solely modified at the OS with PCM (Fig. 5.4a, PCM-kaolinite) or solely modified with D_{16}-*b*-S_{115} at the TS (Fig. 5.4b, D_{16}-*b*-S_{115}-kaolinite) as well as dually modified kaolinite (Fig. 5.4c, D_{16}-*b*-S_{115}/PCM-kaolinite) were recorded in order to demonstrate the modification. Please note that according to the TGA results the total weight fraction of modifiers is less than 5%. Therefore the noise is high.

The spectrum of the PCM-kaolinite (Fig. 5.4a) featured a signal at 16.5 ppm indicating the presence of a CH_3 group of the MMA monomer. Moreover, the $–OCH_3$ group and the CH_2 polymer backbone of PCM could be identified at 44.8 ppm and at 51.5 ppm. Additionally, at 177.1 ppm a signal was detected which is caused by the C=O group of the MMA ester function. The aromatic ring of the catechol function was hardly detectable at 127.1 ppm with small signal-to-noise ratio.

D_{16}-*b*-S_{115}-kaolinite (Fig. 5.4b) featured all the characteristic signals of the neat D_{16}-*b*-S_{115} polymer. At 39.8 ppm and at 44.5 ppm the characteristic CH_2 backbone signals and CH_2 signals of the DMAEMA were recorded. At 127.1 ppm and 146.7 ppm the aromatic CH_1 groups of the styrene could be observed while only a very small signal caused by C=O ester function of the DMAEMA block at 177.1 ppm was detected.

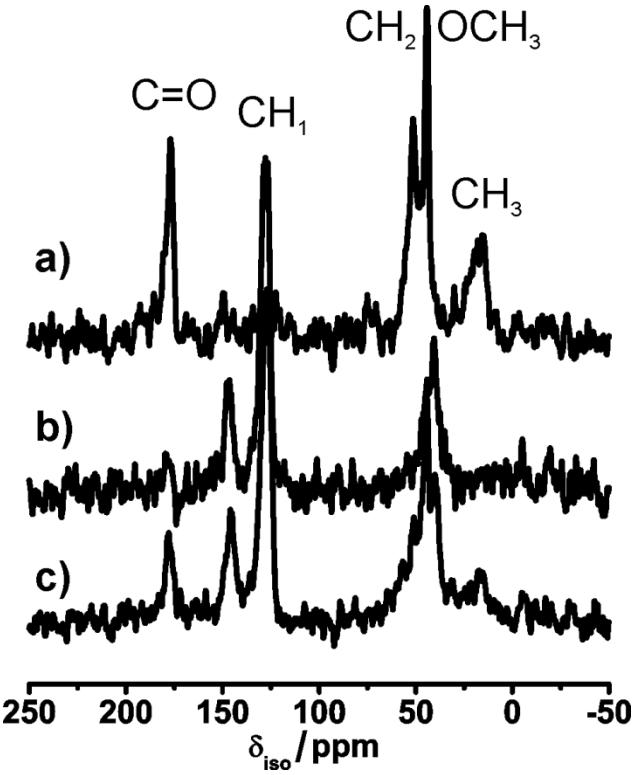

Fig. 5.4 ^{13}C solid-state MAS NMR spectra of a) PCM-kaolinite b) D_{16}-*b*-S_{115}-kaolinite and c) PCM/ D_{16}-*b*-S_{115}-kaolinite.

The spectrum of the D_{16}-*b*-S_{115}/PCM-kaolinite (Fig. 5.4c) represents an overlay of the specific signals of both modifiers indicating that a successful modification with both surface modifiers is feasible. The signals at 16.5 ppm, 51.5 ppm and 177.1 ppm are only or mainly caused by the modification with PCM while the signals at 39.8 ppm, 127.1 ppm and 146.7 ppm could only or mainly be assigned to D_{16}-*b*-S_{115}. Please note that the low loading required very long measurement times (17 h). Therefore, cross-polarization measurement [76] was performed and quantification of signals by integration is impossible. However, the relative intensities of the different signals of each individual modifier (Fig. 5.4a, b) do not change (Fig. 5.4c) indicating that no significant structural changes of the polymer chains occur upon adsorption of the second modifier. This fact in turn would indicate that the adsorption of the two modifiers occurs in a spatially segregated mode as expected given the Janus character.

In summary, modification with PCM and D_{16}-*b*-S_{115} can unequivocally be proven by ^{13}C solid-state NMR, however, due to the very low loading neither quantification nor determination of the ratio between D_{16}-*b*-S_{115} and PCM can be achieved.

Since quantification by NMR was impossible estimating the amount of polymer adsorbed was attempted by TGA. The TGA of pristine kaolinite (Fig. 5.5, pink) features a dehydroxylation to metakaolinite above 410 °C [77] which is accompanied by a mass loss of approximately 13.0 wt%. At 410 °C the modifiers D_{16}-*b*-S_{115} and PCM are, however, already removed as indicated by TGA experiments of mixtures of polymer with inert quartz. Below 410°C pristine kaolinite showed only a minute mass loss of about 0.3 %, probably due to physically adsorbed water which is expected to be completely removed by the surface modification. Consequently, the complete mass loss observed up to a temperature of 410°C may be attributed to the modifiers.

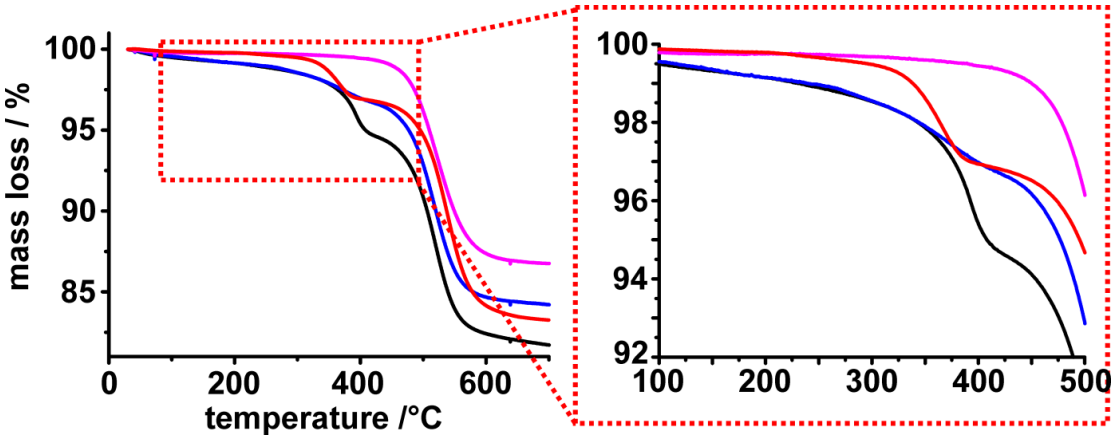

Fig. 5.5 TGA of pristine kaolinite (pink), PCM-kaolinite (blue), D_{16}-*b*-S_{115}-kaolinite (red) and D_{16}-*b*-S_{115}/PCM-modified kaolinite (black).

In the case of the D_{16}-*b*-S_{115}-kaolinite (Fig. 5.5, red) a one-step decomposition with a mass loss of 2.7 wt% starting at 275 °C was observed. In contrast the modifier the PCM-kaolinite (Fig. 5.5, blue) featured a comparatively slow mass loss of 2.7 wt% starting at about 100 °C. The similar overall mass loss for D_{16}-*b*-S_{115}-kaolinite and PCM-kaolinite is of course just coincidental.

The D_{16}-*b*-S_{115}/PCM-kaolinite (Fig. 5.5, black) shows a mass loss of 5% in total, close to the sum of the weight losses of D_{16}-*b*-S_{115}-kaolinite and PCM-kaolinite, indicating that the adsorption of the two modifiers does not influence each other. Moreover, the shape of the TGA-curve of D_{16}-*b*-S_{115}/PCM-kaolinite (Fig. 5.5, black) shows the prominent features of both, D_{16}-*b*-S_{115}-kaolinite and PCM-kaolinite curves.

The experimentally observed loading of D_{16}-*b*-S_{115}-kaolinite may be compared to the loading expected from the CEC of the kaolinite which was around 2.0 mval/100g. Assuming charge neutrality and given that at a pH of ~5.5 approximately 80 % of the DMAEMA monomer units are protonated,[61] a weight content of the D_{16}-*b*-S_{115} in the range of 2.1 wt% of the D_{16}-*b*-S_{115}-kaolinite is expected, slightly less than the experimentally observed mass loss of 2.7 wt%. This difference might be caused either by a lower degree of protonation of the adsorbed D_{16}-*b*-S_{115}.

To verify the selective nature of the dual modification of D_{16}-*b*-S_{115}/PCM-kaolinite indirectly, the stability of the suspension was compared with pristine kaolinite (Fig. 5.6, pink), PCM-kaolinite (Fig. 5.6, blue), and D_{16}-*b*-S_{115}-kaolinite (Fig. 5.6, red). Since the wettability of the samples differs significantly, the experiments were performed in water and in THF.

Please note that in Fig. 5.6 dimeric aggregates are shown rather than intercalation com-pounds. Kaolinite does not form intercalation compounds with polycations, the ion exchange is limited to the tetrahedral external basal surface.

With pristine kaolinite both, TS and OS are highly hygroscopic and consequently suspensions in water were quite stable (Fig. 5.6a, pink), while in THF the stability was very low (Fig. 5.6b, pink).

In contrast, with D_{16}-*b*-S_{115}-kaolinite (Fig. 5.6a, red) the TS was rendered hydrophobic, while the OS remains hydrophilic. Finally, with D_{16}-*b*-S_{115}/PCM-kaolinite the dual modification renders both, TS and OS highly hydrophobic (Fig. 5.6a, black). The aqueous suspensions of both, D_{16}-*b*-S_{115}-kaolinite and D_{16}-*b*-S_{115}/PCM-kaolinite were very unstable. The transparency values in-crease rapidly at early stages of the measurement for both suspensions indicating a high incompatibility between the solvent and the modified kaolinite particles. Apparently, modification of the TS plane makes the whole platelet so hydrophobic, that a ranking regarding the stability of these two suspensions in water, cannot be made because differences observed with these highly unstable suspensions are insignificant.

Surprisingly, in case of the OS-modified PCM-kaolinite (Fig. 5.6a, blue) a high stability of the suspension in water can be achieved which is even comparable with the pristine kaolinite (Fig. 5.6a pink, blue) despite the hydrophobization of the OS. Contrary to D_{16}-*b*-S_{115}-kaolinite where the long PS-brushes extend into the solvent,

the statistical copolymer PCM stays comparatively close to the surface. Moreover, the hydrated inorganic cations residing at unmodified TS contribute to an efficient electrostatic stabilization of PCM-kaolinite in water. Alternatively, the stability of PCM-kaolinite might be explained by the formation of sandwich structures as depicted in Fig. 6a (blue framed inset). For such sandwich structures only the hydrophilic TS are exposed to the aqueous media. Such polymer-bridged sandwich structures would not be expected for D_{16}-*b*-S_{115}-kaolinite because the long PS-brushes will hamper dimer-formation sterically.

In THF (Fig. 5.6b) both, the PCM-kaolinite (Fig. 5.6b, blue) as well as the D_{16}-*b*-S_{115}-kaolinite (Fig. 5.6b, red), showed good stability which in turn is comparable to that of the dually modified D_{16}-*b*-S_{115}/PCM-kaolinite (Fig. 5.6b, black). This suggests that even the short PCM loops at the OS were able to assure a good stability in THF and expectedly the longer chains perform as well. Moreover, it would be expected that sandwich structures of D_{16}-*b*-S_{115}- and PCM-kaolinite are formed (Fig. 5.6b, red and blue squares).

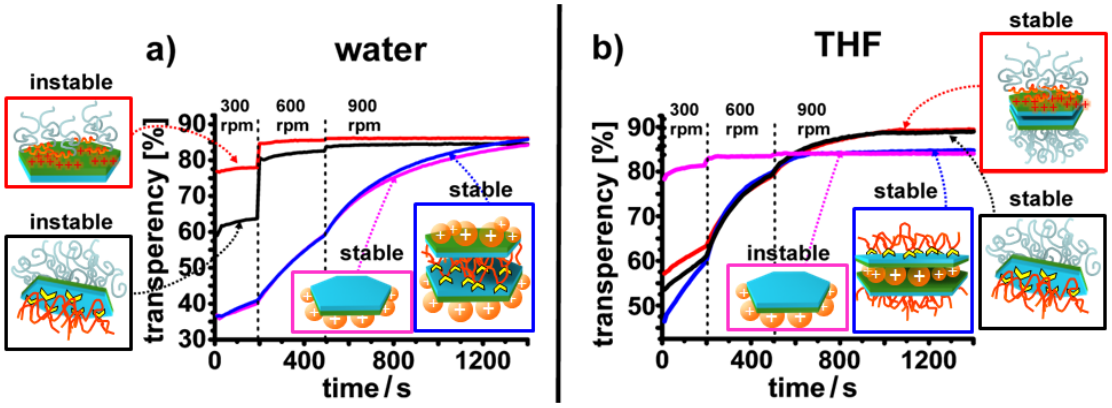

Fig. 5.6 Integrated transparency of 0.25 wt% suspensions in a) water and b) THF of pristine kaolinite (pink), PCM-kaolinite (blue), D_{16}-*b*-S_{115}-kaolinite (red) and D_{16}-*b*-S_{115}/PCM-kaolinite (black) under time dependent centrifugal forces of 300 rpm, 600 rpm, and 900 rpm.

In summary, the stabilities in water- and THF-suspensions observed for the different kaolinite samples are in line with a specific modification of TS and OS by D_{16}-*b*-S_{115} and PCM, respectively, and strongly support the Janus character of D_{16}-*b*-S_{115}/PCM-kaolinite.

5.2 TEM Analysis of the morphology of the hybrid-kaolinite / PMMA/ PS nanocomposites

Dually modified D_{16}-*b*-S_{115}/PCM-kaolinite, where the surface tensions of the opposing basal surfaces are fine-tuned to match PS and PMMA, respectively, was tested as compatibilizer in films of incompatible PS-PMMA blends cast from THF, similar to the process used in chapter 4.3.4. For comparison and to be able to estimate the effect of the Janus character in excess of the pure Pickering effect additional blends with unilaterally modified and blends with unmodified kaolinite were prepared by solvent casting under the same conditions. A PS/PMMA ratio of 1:2 (wt/wt) was chosen.

The samples for transmission electron microscopy (TEM) were prepared by casting the polymer solution with dispersed clay into a glass vial followed by slow drying and microtome cutting. All images are unstained. Dark grey areas result from stronger electron contrast of PS and light grey areas from PMMA. The kaolinite particles appear even darker, almost black, and their shapes are clearly visible due to their strong contrast, the completely white regions are holes in the film, introduced during ultra microtome cutting.

Similar to what was the case with experiments conducted in chapter 4.3.4 we are aware of the fact that solvent evaporation will trap the system in a metastable state and such prepared films can only show the qualitative aspect of compatibilization achieved by our hybrid particles. To determine industrially relevant quantitative effects, like mechanical properties of compatibilized blends, it is necessary to conduct extrusion experiments and mechanical tests.

For pure PS/PMMA blend films of comparable molecular weight that contain no compatibilizers, it is known, that large (several µm in diameter) spherical domains of the minority phase inside a matrix formed by the majority phase result from phase segregation.[51]

With unmodified kaolinite we observe macrophase separation (Fig. 5.7a). No dispersion is achieved, only large aggregates of clay particles can be found, separating from the matrix, trapped inside the polymer phase where they happen to be upon drying (Fig. 5.7a). This behaviour is expected due to the clay's hydrophilic

nature (charged on one side and polar hydroxy groups on the other side) and the fact that it does not form stable dispersions in THF (and thus is hard to disperse in the Polymer mixture to start with). In another experiment we modified the TS of kaolinite with dodecylamine, which is comparable in structure to the alkyl ammonium salts used to prepare commercial organoclay like the widely used Cloisite 20A. Here we can observe clustering in the PMMA phase (Fig. 5.7b). Like in the Lumifuge experiments we expect the kaolinite to form sandwich structures with the alkyl chains of the organophilized TS aggregated via hydrophobic interactions in the inside and the polar OS at the outside or the other way round. In none of the cases we could find a surface which has high compatibility with any of the polymer phases and thus is not dispersed homogeneously. This observation is in good agreement with literature about other organoclay (e.g. Cloisite 20A), which disperses only in the PMMA phase of a PS/PMMA blend and forms strong clusters in PS homopolymer blends.[75] Obviously modification of one side is not sufficient to align the particles at the interface under these conditions.

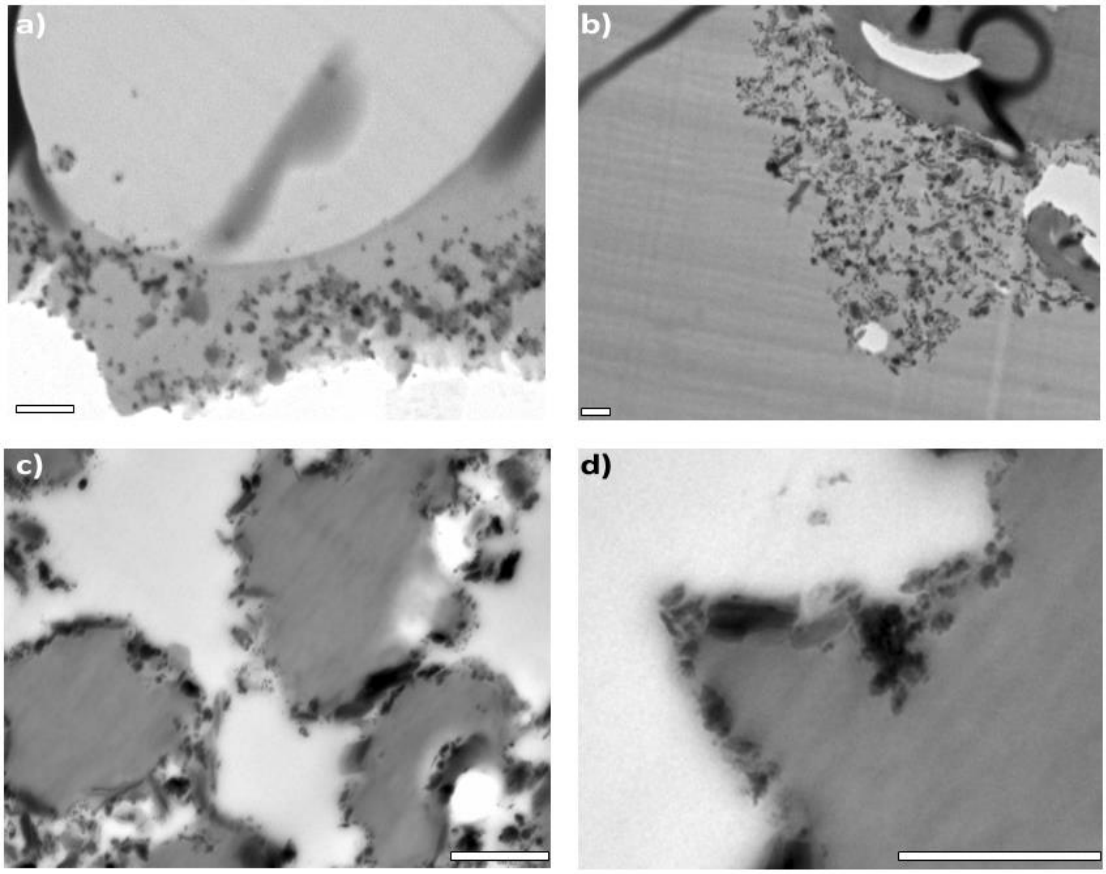

Fig. 5.7 TEM images of 3:7 (wt/wt) PS/PMMA blend films. a) with pristine kaolinite, b) with unilaterally organophilized kaolinite, c) with D_{16}-*b*-S_{115}/PCM-kaolinite, and d) close up at an inter-face. The fraction of the clay is 5wt% and the scale bar represents 500 nm.

In contrast, in the film prepared with the Janus-type D_{16}-*b*-S_{115}/PCM-kaolinite (Fig. 5.7c, d) the kaolinite particles are assembled exactly at the interface between both polymer phases. A nearly full coverage of the interface by compatibilizer is realized. Due to the Janus character of the modified kaolinite the interfacial tension of the platelets in the blend interface should be very low. Therefore, the assembly of the particles at the interface is energetically highly favored. As a consequence, the PS domains are no longer spherical but appear polygonal following the shape of the clay platelets (Fig. 5.7c, d).

5.3 Conclusion

A synopsis of all experimental data presented confirms that the external basal planes of kaolinite platelets can be selectively addressed by polystyrene and PMMA, similar to what has been studied in detail for the molecular modification with $Ru(bpy)_3^{2+}$ and a phosphorous-labelled catechol (3-Diphenylphosphinyloxypropyl-3,4-dihydroxybenzoate) in literature[21]. Janus-type D_{16}-*b*-S_{115}/PCM-kaolinite platelets obtained by dual modification showed interfacial activity in a solvent-cast PS/PMMA blend film. Obviously, blend preparation via melt extrusion would be advantageous. Work in that direction is on the way but the results obtained by solvent-casting already give a strong indication on the efficiency of the hybrid Janus particles as blend compatibilizers.

While the presented work represents a proof of principle, the approach is, of course, highly modular and should allow for facile and affordable fine-tuning of appropriate compatibilizers for a broad range of blend systems.

The intrinsically polar structure of kaolinite serves as versatile core of these Janus platelets. Adjustment of the surface tensions of both basal planes can easily and selectively be tailored for each specific blend composition. Moreover, particle size distribution and morphology (aspect ratio) may be varied over a wide range by the choice of the kaolinite source. Furthermore, that concept is not restricted to kaolinite but can be transferred to any other inorganic material which possesses a polar crystal structure and where opposing crystal faces are truncated by chemically different functional groups, paving the way to selective modification.

An additional advantage of the concept should be an inherent reinforcement of the blend by the inorganic filler, which, moreover, is concentrated at the blends interfaces. This should create a synergistic effect stretching far beyond a pure Pickering effect and should boost the mechanical properties of the blend.

Chapter 6: References

1. Hussain, F.; Hojjati, M.; Okamoto, M.; Gorga, R. E., *Journal of Composite Materials* **2006,** 40, (17), 1511-1575.

2. Gary W. Beall, C. E. P., *Fundamentals of Polymer-Clay Nanocomposites*. Cambridge University Press: 2011.

3. Brigatti, M. F.; Galan, E.; Theng, B. K. G.; Fayza Bergaya, B. K. G. T. a. G. L., Chapter 2 Structures and Mineralogy of Clay Minerals. In *Developments in Clay Science*, Elsevier: 2006; Vol. Volume 1, pp 19-86.

4. Breu, J., *Tone und Tonminerale*. Universität Bayreuth: 2007.

5. Ralph, J., http://www.mindat.org/min-2821.html. In 14.12.2012.

6. J. Breu, N. R., C. R. A. Catlow, *J.Chem.Soc.Dalton Trans.* **1999**, 835-845.

7. J. Breu, N. R., C. R. A. Catlow, in Natural Microporous Materials in; Environmental Technology , V., (Eds.: P. Misaelides, F. Macasek, T.; Pinnavaia, C. C., Kluwer Academic Publishers, Dordrecht 1999, p. pp.; 85-99.

8. Sato, H.; Yamagishi, A.; Kawamura, K., *The Journal of Physical Chemistry B* **2001,** 105, (33), 7990-7997v.

9. Strawhecker, K.; Manias, E., *Chem. Mater.* **2000,** 12, 2943.

10. Vaia, R.; Vasudevan, S.; Krawiec, W.; Scanlon, L. G.; Giannelis, E. P., *Adv. Mater.* **1995,** 7, 154.

11. Alexandre, M.; Dubois, P., *Materials Science and Engineering: R: Reports* **2000,** 28, (1-2), 1-63.

12. Schmidt, D.; Shah, D.; Giannelis, E. P., *Current Opinion In Solid State & Materials Science* **2002,** 6, (3), 205-212.

13. Kalo, H.; Möller, M. W.; Ziadeh, M.; Dolejs, D.; Breu, J., *Applied Clay Science* **2010,** 48, (1-2), 39-45.

14. Weiss, S.; Hirsemann, D.; Biersack, B.; Ziadeh, M.; Müller, A. H. E.; Breu, J., *Polymer* **2013**, (0).

15. Chevigny, C.; Jouault, N.; Dalmas, F.; Boue, F.; Jestin, J., *Journal of Polymer Science Part B: Polymer Physics* **2011,** 49, (11), 781-791.

16. Neder, R. B.; Burghammer, M.; Grasl, T.; Schulz, H.; Bram, A.; Fiedler, S., *Clays and Clay Minerals* **1999,** 47, (4), 487-494.

17. Wada, K., *American Mineralogist* **1961,** 46, (1-2), 78-91.

18. Komori, Y.; Sugahara, Y.; Kuroda, K., *Journal of Materials Research* **1998,** 13, (4), 930-934.

19. Brady, P. V.; Cygan, R. T.; Nagy, K. L., *Journal Of Colloid And Interface Science* **1996,** 183, (2), 356-364.

20. Schroth, B. K.; Sposito, G., *Clays and Clay Minerals* **1997,** 45, (1), 85-91.

21. Hirsemann, D.; Shylesh, S.; De Souza, R. A.; Diar-Bakerly, B.; Biersack, B.; Mueller, D. N.; Martin, M.; Schobert, R.; Breu, J., *Angewandte Chemie International Edition* **2012,** 51, (6), 1348-1352.

22. Inoue, M.; Kominami, H.; Inui, T., *Journal Chemical Society Dalton Transactions* **1991**, (12), 3331-3336.

23. Inoue, M.; Kondo, Y.; Inui, T., *Inorganic Chemistry* **1988,** 27, (2), 215-221.

24. Henglein, A., *Chemical Reviews* **1989,** 89, (8), 1861-1873.

25. Spanhel, L.; Weller, H.; Henglein, A., *Journal of the American Chemical Society* **1987,** 109, (22), 6632-6635.

26. Youn, H. C.; Baral, S.; Fendler, J. H., *The Journal of Physical Chemistry* **1988,** 92, (22), 6320-6327.

27. Hoener, C. F.; Allan, K. A.; Bard, A. J.; Campion, A.; Fox, M. A.; Mallouk, T. E.; Webber, S. E.; White, J. M., *The Journal of Physical Chemistry* **1992,** 96, (9), 3812-3817.

28. Honma, I.; Sano, T.; Komiyama, H., *The Journal of Physical Chemistry* **1993,** 97, (25), 6692-6695.

29. Zhou, Z. H.; Gunter, W. D., *Clays and Clay Minerals* **1992,** 40, (3), 365-368.

30. Hofman-Caris, C. H. M., *New Journal of Chemistry* **1994**, (18), 1087.

31. Ruhland, T. M.; Reichstein, P. M.; Majewski, A. P.; Walther, A.; Müller, A. H., *J Colloid Interface Sci* **2012,** 374, (1), 45-53.

32. Gröschel, A. H.; Schacher, F. H.; Schmalz, H.; Borisov, O. V.; Zhulina, E. B.; Walther, A.; Müller, A. H. E., *Nat Commun* **2012,** 3, 710.

33. Schmelz, J.; Karg, M.; Hellweg, T.; Schmalz, H., *ACS Nano* **2011,** 5, (12), 9523-9534.

34. Pawar, A. B.; Kretzschmar, I., *Macromolecular Rapid Communications* **2010,** 31, (2), 150-168.

35. Schmelz, J., Dissertation, University of Bayreuth, 2012.

36. Walther, A.; Muller, A. H. E., *Soft Matter* **2008,** 4, (4), 663-668.

37. Casagrande, C.; Veyssié, M., *C.R. Acad. Sci. (Paris)* **1988,** Ser II, (306), 1423.

38. Casagrande, C.; Veyssié, M.; Fabre, P.; Raphael, E., *Europhys. Lett.* **1989,** 9, (3), 251-255.

39. Nisisako, T.; Torii, T.; Takahashi, T.; Takizawa, Y., *Advanced Materials* **2006,** 18, (9), 1152-1156.

40. Behrend, C. J.; Anker, J. N.; McNaughton, B. H.; Kopelman, R., *Journal of Magnetism and Magnetic Materials* **2005,** 293, (1), 663-670.

41. Anker, J. N.; Behrend, C. J.; Huang, H.; Kopelman, R., *Journal of Magnetism and Magnetic Materials* **2005,** 293, (1), 655-662.

42. Yoshida, M.; Roh, K.-H.; Mandal, S.; Bhaskar, S.; Lim, D.; Nandivada, H.; Deng, X.; Lahann, J., *Advanced Materials* **2009,** 21, (48), 4920-4925.

43. Kojima, Y.; Usuki, A.; Kawasumi, M.; Okada, A.; Fukushima, Y.; Kurauchi, T.; Kamigaito, O., *Journal of Materials Research* **1993,** 8, (5), 1185-1189.

44. Okada, A.; Usuki, A., *Materials Science and Engineering: C* **1995,** 3, (2), 109-115.

45. Rockwood, http://www.nanoclay.com/benefits2.asp. In 14.12.2012.

46. Short, G. J.; Guild, F. J.; Pavier, M. J., *Composites Science and Technology* **2001,** 61, (14), 2075-2086.

47. Ruckdäschel, H.; Sandler, J. K. W.; Altstädt, V.; Rettig, C.; Schmalz, H.; Abetz, V.; Müller, A. H. E., *Polymer* **2006,** 47, (8), 2772-2790.

48. Binks, B. P.; Lumsdon, S. O., *Langmuir* **2001,** 17, (15), 4540-4547.

49. Nesterov, A. E.; Lipatov, Y. S., *Polymer* **1999,** 40, (5), 1347-1349.

50. Khatua, B. B.; Lee, D. J.; Kim, H. Y.; Kim, J. K., *Macromolecules* **2004,** 37, (7), 2454-2459.

51. Li, Y.; Shimizu, H., *Polymer* **2004,** 45, (22), 7381-7388.

52. Li, Y. Q.; Zhang, G.; Nurmikko, A. V.; Sun, S. H., *Nano Letters* **2005,** 5, (9), 1689-1692.

53. Ammann, L.; Bergaya, F.; Lagaly, G., *Clay Minerals* **2005,** 40, (4), 441-453.

54. Cai, Y.; Armes, S. P., *Macromolecules* **2004,** 38, (2), 271-279.

55. Keller, W., *Applied Clay Science* **2008,** 5, 123-133.

56. Möller, M. W.; Handge, U. A.; Kunz, D. A.; Lunkenbein, T.; Altst„dt, V.; Breu, J., *Acs Nano* **2010,** 4, (2), 717-724.

57. Wang, W.-L.; Chai, S. C.; Ye, Q.-Z., *Bioorganic & Medicinal Chemistry Letters* **2009,** 19, (4), 1080-1083.

58. Bottcher, H.; Hallensleben, M. L.; Nuá, S.; Wurm, H.; Bauer, J.; Behrens, P., *Journal of Materials Chemistry* **2002,** 12, (5), 1351-1354.

59. Matyjaszewski, K.; Miller, P. J.; Shukla, N.; Immaraporn, B.; Gelman, A.; Luokala, B. B.; Siclovan, T. M.; Kickelbick, G.; Vallant, T.; Hoffmann, H.; Pakula, T., *Macromolecules* **1999,** 32, (26), 8716-8724.

60. Carrado, K. A.; Decarreau, A.; Petit, S.; Bergaya, F.; Lagaly, G.; Bergaya, F.; Benny, K. G., Chapter 4 Synthetic Clay Minerals and Purification of Natural Clays. In

Developments in Clay Science Handbook of Clay Science, Elsevier: 2006; Vol. 1st ed., pp 115-139.

61. Plamper, F. A.; Ruppel, M.; Schmalz, A.; Borisov, O.; Ballauff, M.; Müller, A. H. E., *Macromolecules* **2007,** 40, (23), 8361-8366.

62. Oral, A.; Shahwan, T.; Guler, C., *Journal of Materials Research* **2008,** 23, (12), 3316-3322.

63. Wang, B. X.; Zhao, X. P., *Journal of Materials Chemistry* **2003,** 13, (9), 2248-2253.

64. Hwang, S. J.; Chen, C. Y.; Zones, S. I., *Journal Of Physical Chemistry B* **2004,** 108, (48), 18535-18546.

65. Yamamoto, S.; Ejaz, M.; Tsujii, Y.; Fukuda, T., *Macromolecules* **2000,** 33, (15), 5608-5612.

66. Madejova, J.; Keckes, J.; Paalkova, H.; Komadel, P., *Clay Minerals* **2002,** 37, (2), 377-388.

67. Ejaz, M.; Tsujii, Y.; Fukuda, T., *Polymer* **2001,** 42, (16), 6811-6815.

68. Husseman, M.; Malmstr”m, E. E.; McNamara, M.; Mate, M.; Mecerreyes, D.; Benoit, D. G.; Hedrick, J. L.; Mansky, P.; Huang, E.; Russell, T. P.; Hawker, C. J., *Macromolecules* **1999,** 32, (5), 1424-1431.

69. Fischer, B.; Ziadeh, M.; Pfaff, A.; Breu, J.; Altst„dt, V., *Polymer* **2012,** 53, (15), 3230-3237.

70. Liaw, J. H.; Hsueh, T. Y.; Tan, T. S.; Wang, Y.; Chiao, S. M., *Polymer International* **2007,** 56, (8), 1045-1052.

71. Meneghetti, P.; Qutubuddin, S., *Thermochimica Acta* **2006,** 442, (1â€“2), 74-77.

72. Shin, Y. W.; Roberts, J. E.; Santore, M., *Journal of Colloid and Interface Science* **2001,** 244, (1), 190-199.

73. Arita, T.; Buback, M.; Vana, P., *Macromolecules* **2005,** 38, (19), 7935-7943.

74. Russell, T. P.; Hjelm, R. P.; Seeger, P. A., *Macromolecules* **1990,** 23, (3), 890-893.

75. Yang, S. M.; Kim, S. H.; Lim, J. M.; Yi, G. R., *Journal of Materials Chemistry* **2008,** 18, (19), 2177-2190.

76. Levitt, M. H.; Raleigh, D. P.; Creuzet, F.; Griffin, R. G., *The Journal of Chemical Physics* **1990,** 92, (11), 6347-6364.

77. Rocha, J.; Klinowski, J., *Angewandte Chemie-International Edition In English* **1990,** 29, (5), 553-554.

Acknowledgements

It is needless to say, that this work would have been impossible without the help of several great people. I would like to use this as an opportunity to say thank you to all of them.

First of all, I want to thank Prof. Dr. Axel H. E. Müller for the warm welcome in his department, his continued support during my work and the enormous freedom left to all of us. I have to thank him for suggesting the topic of this thesis, it surely was not always a delight to be working on, but it taught me a lot and forced me to develop myself, academically as well as personally. Finally I want to thank him for the unique experiences presented through participation in conferences and seminars all around the world.

I want to thank my lab mates Thomas Ruhland, Markus Müllner and André Gröschel and all of the rest of MCII group, whose diverse and lovely characters made up the unique charm of this chair. Their great spirit has always driven me to work and sometimes certainly stopped me from it as well. Even if the research did not always run as smoothly as planned, every day spent in MCII was a good day nevertheless. Special thanks to Gaby Oliver for making university live as easy and unbeaurocratic as possible.

My special gratefulness goes to Melanie, Annika and Marietta for their excellent measurements and technical support with all things related to electron microscopy and size exclusion chromatography. Thanks to Annette for keeping us safe as well. I also have to thank all my labcourse students, Sabrina Kerling, Christian Bartz, Fabian Nutz, Fabian Pooch, Andreas Edenhardter, Georg Schlageter, Phillip Knauer and Hannes Heigl for their practical work under my supervision

I have to thank Prof. Breu for taking me on after our chair had been taken over and for his support during my thesis. Thanks to Dunja Hirsemann for cooperating on the work on kaolinite and setting the base for creating a real Janus particle from it. My special thanks goes to Mazen Ziadeh for not only cooperating on all things related to inorganic matter, but for sharing the good and bad times during labwork, especially in the last part of the thesis, as well and keeping me motivated regardless of results.

Acknowledgements

Thanks to everyone else who contributed to this unforgettable time I had during my life in Bayreuth, especially my crazy flatmates, Küken, Kim, Sophia, Daniel, Paul and Malte, my dear friends Ludger and Lukas, my latest squeeze Isabel, my hobby soccer Team Freudenhaus and everyone else I had the pleasure to meet through couch surfing, campus Kandinsky, Gründerforum, Bayreuth's night life and sports.

My deepest gratitude goes to my parents for always believing in me, regardless of what I do. I have to apologize to my grandfather for taking so long to write my thesis. Finally, I want to thank the rest of my big, wonderful family for inspiring me by their positive way of thinking, no matter what happens.

Erklärung

Die vorliegende Arbeit wurde von mir selbstständig verfasst, und ich habe dabei keine anderen als die angegebenen Hilfsmittel und Quellen benutzt.

Ferner habe ich nicht versucht, anderweitig mit oder ohne Erfolg eine Dissertation einzureichen oder mich der Doktorprüfung zu unterziehen.

Bayreuth, den _____

Stephan Weiß